Risk and resilience-based optimal post-disruption restoration for critical infrastructures under uncertainty

Basem A. Alkhaleel[a], Haitao Liao[a,*], Kelly M. Sullivan[a]

[a]*Department of Industrial Engineering, University of Arkansas, Fayetteville, AR 72701, USA*

Abstract

Post-disruption restoration of critical infrastructures (CIs) often faces uncertainties associated with the required repair tasks and the related transportation network. However, such challenges are often overlooked in most studies on the improvement of CI resilience. In this paper, two-stage risk-averse and risk-neutral stochastic optimization models are proposed to schedule repair activities for a disrupted CI network with the objective of maximizing system resilience. Both models are developed based on a scenario-based optimization technique that accounts for the uncertainties of the repair time and the travel time spent on the underlying transportation network. Given the large number of uncertainty realizations associated with post-disruption restoration tasks, an improved fast forward algorithm based on a wait-and-see solution methodology is provided to reduce the number of chosen scenarios, which results in the desired probabilistic performance metrics. To assess the risks associated with post-disruption scheduling plans, a conditional value-at-risk (CVaR) metric is incorporated into the optimization models through a scenario reduction algorithm. The proposed restoration framework is applied to the French RTE electric power network with a DC power flow procedure, and the results demonstrate the added value of using the stochastic optimization models incorporating the travel times related to repair activities. It is essential that risk-averse decision-making under uncertainty largely impacts the optimum schedule and the expected resilience, especially in the worst-case scenarios.

Keywords: (O) OR in disaster relief; Stochastic optimization; Restoration; Risk measures

1. Introduction

1.1. Background

Critical infrastructures (CIs) are defined as networks of independent, mostly privately-owned, man-made systems and processes that function collaboratively and synergistically to produce and distribute a continuous flow of essential goods and services (Ellis et al., 1997). Specially, those CI networks for electric power, water distribution, natural gas, transportation, and telecommunications are the backbone of modern societies (Almoghathawi et al., 2019; Zio, 2016). Their continuous and proper functioning provides the fundamental services that support the economic productivity, security, and quality of life of citizens.

*Corresponding author:
Email address: liao@uark.edu (Haitao Liao)

Unfortunately, CI networks are often subject to different types of disruptive events, including random failures, technical accidents, malevolent attacks, and natural hazards, which could affect their performance unpredictably and have direct consequences on the communities and people's daily lives. Such disruptions become inevitable in today's increasingly complex and risky operating environment (Helbing, 2013). Hence, for several years, the United States (U.S.), as well as many countries around the globe, have shown an increasing interest in effectively preparing for and responding promptly to such disruptive events (Karagiannis et al., 2017; O'Donnell, 2013; White House, 2013). Indeed, it is increasingly important to not only protect the current CI networks against disruption, but also to be able to restore them once they are disrupted.

In 2011, the U.S. president released a report setting a four-pillared strategy for modernizing the electric grid (Executive Office of the President, 2011). The presidential initiative directed billions of dollars toward the investments in 21st century smart grid technologies aiming at increasing the grid's efficiency, reliability, and resilience, and at making the grid less vulnerable to outages and reducing the time it takes to restore power after an outage. A subsequent report in 2013 has addressed explicitly the importance of increasing electric grid resilience, especially against weather-related outages, and the economic benefits of resilience improvement (Executive Office of the President, 2013). According to the report, severe weather is the leading cause of power outages in the U.S. In fact, between 2003 and 2012, an estimated 679 widespread power outages occurred due to severe weather. Such weather-outages are expected to rise as climate change increases the frequency and intensity of hurricanes, blizzards, floods, and other extreme weather events (Zamuda et al., 2013). In addition, weather-related outages are estimated to have cost the U.S. economy an inflation-adjusted annual average of $18 billion to $33 billion (Executive Office of the President, 2013). The annual estimation could reach $70 billion according to another congressional study (Campbell & Lowry, 2012).

It is worth pointing out that the annual losses fluctuate significantly and reach the greatest in the years of major storms. For example, Hurricane Sandy, which struck the entire East Coast of the U.S. in October 2012, caused significant damages to the infrastructure systems, resulting in an estimated cost of $33 billion for repairs and cleanup in the aftermath and an approximate total of $65 billion in damages and economic loss (Force, 2013). Moreover, about 8.5 million customers were left without power, and the commuting time increased significantly due to the disabled roads and public transit. When Hurricane Harvey struck the southern coast, it caused about $200 billion in damages and $20 to $30 billion in lost economic output (CNBC, 2017). According to the U.S. Federal Emergency Management Agency (FEMA), nearly 40,000 people were in the shelters in Texas and Louisiana, considering the most were without essential lifeline services, over 160 drinking water systems were damaged with 50 of them being totally shut down, and 800 water waste facilities were partially damaged (FEMA, 2017). Furthermore, nearly 80,000 homes had at least 18 inches of floodwater, 23,000 of which had more than 5 feet, 24 hospitals were evacuated, 61 communities lost drinking water capability, 23 ports were closed, 781 roads were impassable, about 780,000 people evacuated their homes, and first responders rescued 122,331 people (FEMA, 2017). Altogether, the experience from these events underlines the needs for timely, efficient, and effective network restoration and recovery activities in the aftermath of large-scale disruptive events, so that both short-term and long-term reliance on the infrastructure networks can be assured.

Risk management strategies generally emphasize disruptive events mitigation options in the form of prevention and protection by designing the systems to avoid or absorb undesired events from occurring (Hosseini et al., 2016). While such strategies are crucial to preventing undesired events or consequences, recent events suggest that not all undesired events can be prevented. Natural events such as Hurricane Harvey are among the recent examples of unpreventable disruptions. In fact, this particular event impacted multiple networked systems including the transportation network and power network, which has not been restored fully even after few months of the incident (Manuel, 2013). In a recent report by the European Commission's science and knowledge service, the Joint Research Centre (JRC) has addressed challenges in power grid recovery after natural hazards (Karagiannis et al., 2017). The study covered different natural events and their impact on power grid networks by collecting worldwide data about at least 50 events from different sources including technical reports, field survey reports, and research papers (Karagiannis et al., 2017). The report used two thresholds to assess power grid recoverability: (1) The restoration of power supply to customers, and (2) The complete repair of the network. Moreover, two of the significant challenges that face recovery actions were found to be the repair times uncertainty and poor access to damaged facilities due to landslides or traffic congestions. In addition, the report was concluded with multiple recommendations to improve power grid recovery ranging from integrating risk-related strategies to stockpiling spare parts for urgent maintenance actions (Luo et al., 2020).

All such recovery planning actions after disruptions are part of the rising concept of resilience, which can be defined generally as the ability of a system or an organization to react and recover from unanticipated disturbances and events (Hollnagel et al., 2006). Resilience, and in particular CI resilience, has emerged in recent years due to the awareness of governments about the possible risks associated with CIs and the catastrophic impacts of various disruptive events affecting CIs (White House, 2013). This has encouraged practitioners and researchers to develop various resilience improvement techniques ranging from system design to recovery optimization (Hosseini et al., 2016). In addition, resilience can be effectively improved by developing optimum plans for timely restoring the disrupted service after the occurrence of a disruptive event. In planning CIs restoration, prioritizing components is key in improving the recovery process. To this end, optimization approaches are typically used to facilitate the identification and scheduling of effective restoration strategies for the rapid reestablishment of system functionality. Recently, Sharkey et al. (2020) reviewed the relation between network optimization and resilience theory and applications. In the literature, many studies have been reported in the context of post-disruption CI restoration under a mathematical programming framework (Fang & Sansavini, 2017; Nurre & Sharkey, 2014; Vugrin et al., 2014; Zhang et al., 2018). The main goal is to schedule recovering tasks of failed components in order to accelerate the restoration process (Vugrin et al., 2014).

1.2. Related literature

The concept of resilience has been investigated by different disciplinary perspectives and across various application domains. Specially, several definitions of resilience have been offered from an engineering point of view (Hosseini et al., 2016). Many are similar and overlap with a number of existing concepts such as robustness, fault tolerance, flexibility, survivability, and agility, among others. However, most definitions are based around pre- and post-disruption related concepts, such as protection,

risk mitigation, adaption and restoration (Barker et al., 2017). In addition, developing mathematical and statistical modeling approaches to improve, analyze and optimize resilience needs resilience quantification to compare proposed models. As a result, in the literature, resilience has been quantified by different approaches and mathematical interpretations (Gasser et al., 2019; Hosseini et al., 2016). Many of these resilience measures try to scale the performance measure as a ratio between the actual level of performance and the desired (undisrupted) level over time (for a full review see Gasser et al. (2019) and Hosseini et al. (2016)). Some examples are the ratio of the probability of failure and recovery (Li & Lence, 2007), the ratio of the expected degradation and the maximum possible degradation of a system due to a disruption (Rose, 2007), and the measure of system performance (Henry & Ramirez-Marquez, 2012). In this work, the focus will be on post-event resilience-based actions (i.e., restoration and/or recovery).

There are multiple studies addressing post-disruption CI restoration with different goals and mathematical approaches. Anaya-Arenas et al. (2014) and Özdamar & Ertem (2015) reviewed post-disruption restoration plans in humanitarian logistics, such as relief delivery, casualty transportation, and mass evacuation. In addition, considerable research in this area has been focused on specific types of critical infrastructures such as transportation networks and electrical power grids (Morshedlou, 2018). In contrast, other studies developed general restoration models that can be applied to almost any CI network without changes or with slight modifications (e.g., adding power flow constraints in power grids). Although the literature review will not be restricted to one type of CIs models, restrictions associated with a single CI model will be mentioned.

Many of the mathematical models found in the literature are formulated as mixed integer programs (MIPs) and mixed integer linear programs (MILPs). Bryson et al. (2002) applied an MIP approach for selecting a set of recovery subplans leading to the greatest benefit to business operation. Matisziw et al. (2010) proposed an MIP model to restore networks where the connectivity between pairs of nodes is considered as the performance measure associated with the network. Nurre et al. (2012) studied an integrated network design and scheduling problem for the restoration of CI systems. They formulated the problem as an integer programming problem, and a dispatch rule-based heuristic approach was proposed for its efficient solution. To account for power flow law in electrical networks, they adopted the method by Bienstock & Mattia (2007). Furthermore, Nurre & Sharkey (2014) provided a comparative study focusing mainly on model complexity and heuristic dispatch rules for their integer optimization problem.

Regarding cascading failures in power networks, Bienstock & Mattia (2007) proposed an MIP model to protect power grid networks at minimum costs to increase the networks survivability against cascading failures. Their DC power flow model can be implemented in general MIPs and MILPs by just adding a small set of constraints to control the power flow. To control power transmission networks, Chang & Wu (2011) explored a quantitative method to measure the stability and reliability of electric power networks under the triggered cascading failures. In addition, Bienstock & Grebla (2015) introduced a stochastic algorithm to minimize the lost power load at the termination of the cascade considering noise and errors in the model. Fang et al. (2017) introduced a pattern for searching for the optimal limited resource allocation to increase the capacity of some links in electric power networks to be able to maximize the networks resistance to cascading failures.

Multiple infrastructures restoration models can also be found in the literature. Casari & Wilkie (2005) discussed multiple infrastructures restoration when CIs are operated by different firms. Lee II et al. (2007) proposed an MIP model to minimize the operating costs for temporary emergency restoration, where network restoration involves selecting the locations of temporary arcs needed to completely reestablish network services over a set of interdependent networks. Ouyang & Wang (2015) studied and compared the effectiveness of five strategies for joint restoration of interdependent infrastructures, and a Genetic Algorithm (GA) was applied to generate recovery sequences. Sharkey et al. (2015) studied the restoration of multiple interdependent CI networks under a centralized decision-making framework and suggested an MIP model to solve the problem. Furthermore, González et al. (2016) proposed an MIP model for optimizing infrastructure system restoration considering joint restoration due to the geographical interdependence between multiple CI systems. Recently, Garay-Sianca & Pinkley (2021) studied the restoration of interdependent CIs considering the movement of work crews through a damaged transportation network being restored and proposed an MIP to solve the problem under a deterministic problem setting.

When only transportation networks are concerned, Aksu & Ozdamar (2014) considered a multi-vehicle problem to maximize network accessibility during transportation network recovery by identifying critical blocked links and restoring them with limited resources. Çelik et al. (2015) also considered debris removal problems and developed a stochastic debris removal approach over discrete time periods to determine the optimal schedule of blocked links under uncertainty. It was assumed that the information corresponding to clearance time changes as the amount of debris changes, and thus as the information is updated, the restorative vehicles assignment schedule changes. Furthermore, Kasaei & Salman (2016) studied arc routing problems to regain network connectivity by clearing blocked roads, developing heuristic algorithms to attain the maximum benefit gained by network connectivity while minimizing the time horizon. Recently, Iloglu & Albert (2020) proposed a restoration model of transportation networks to deliver critical services after disasters by heuristically optimizing the relocation process of emergency responders to maximize the coverage of emergency services demand over time.

One can see that the vast majority of these studies are based on deterministic assumptions such as complete information on the restoration resources and full knowledge of the activities durations. However, the restoration of infrastructure systems is complicated by the many decisions to be made in a highly uncertain environment exacerbated by the disaster itself, people's reaction, and limited capability of information gathering (Fang & Sansavini, 2019). Several factors introduce uncertainty into the parameters of a disaster situation, e.g., availability of restoration resources, number of repair crews, the time duration for repairing failed components and the accessibility to such failed components through the related transportation network. Clearly, optimal task planning under uncertainty appears to be the closest to a real-life situation. In addition, existing optimization approaches usually do not account for risk measures related to the execution of the optimal plan. For example, if the time durations of some repair activities were longer than expected, the doubt would be if the suggested plan will still perform well. Obviously, when optimizing CI restoration, risks associated with the restoration plan must be considered to identify the possible worst-case scenarios and alter the plan accordingly. Furthermore, the travel time between failed components may also affect the proposed

plan along with the accessibility of components under the transportation network condition.

In the literature, few studies have tackled uncertainty in post-disruption CI restoration. Xu et al. (2007) optimized a power network restoration by scheduling inspection, assessment, and repair operations, which were assumed to have random durations with known probability distributions. Instead of solving the stochastic model, the authors used a GA to produce a priority list of repair tasks, which might be suboptimal. Recently, Fang & Sansavini (2019) proposed a stochastic optimization approach for infrastructure restoration under uncertainty and showed the added value of the stochastic model compared to the deterministic counterpart. However, risk measures, the effects of travel time and the impact of different network failure modes were not considered in their model.

1.3. Overview and research contributions

The aim of this paper is to schedule restoration actions on failed CI components using multiple maintenance crews by solving a two-stage stochastic optimization model. The first stage schedules repair tasks, and the second stage resolves the CI performance for each time period. The scheduled tasks have uncertain duration, and the travel times between different tasks are also uncertain. Considering these sources of uncertainty, two variants of the proposed stochastic optimization model are: (1) a risk-neutral model to optimize restoration activities accounting for uncertainty and (2) a conditional value-at-risk (CVaR)-based risk-averse model that enables the decision maker to choose plans that perform well even in worst-case scenarios.

The main contributions of this paper are three-fold. (1) To the best of our knowledge, this is the first paper that incorporates risk measures into resilience-based optimization in the context of post-disruption restoration; (2) it provides a general framework for the generation, selection and reduction of scenarios based on an improved fast forward selection algorithm for resilience optimization; and (3) it provides the first stochastic optimization models that account for the travel time between failed components for post-disruption restoration.

The remainder of this paper is organized as follows. Section 2 presents the background and methodology pertinent to our models and summarizes the proposed mathematical formulations. Section 3 shows the solution approach used in this paper. Section 4 presents a case study on the RTE electric power network to illustrate the use and advantage of the suggested models. Finally, concluding remarks and future research directions are provided in Section 5.

2. Methodology and model development

2.1. Resilience of critical infrastructure

The resilience of a CI is commonly characterized with respect to a measure of performance (e.g., flow, connectivity, amount of demand satisfied) $\varphi(t)$ that evolves over time (Henry & Ramirez-Marquez, 2012; Hosseini et al., 2016). As depicted in Figure 1, let $t_e \leq t_d \leq t_s \leq t_f$ denote instants in time such that (i) a disruptive event occurs at time t_e causing $\varphi(t)$ to begin decreasing; (ii) the effects of the disruption are fully realized at time t_d, causing $\varphi(t)$ to stop decreasing; (iii) recovery of the CI begins at time t_s, causing $\varphi(t)$ to begin increasing; and (iv) recovery of the CI is complete at time t_f, causing $\varphi(t)$ to stop increasing.

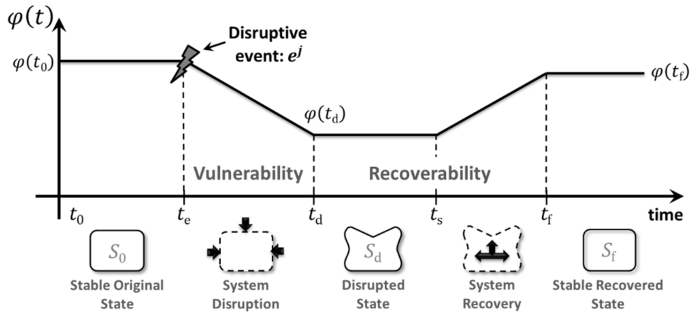

Figure 1: Illustration of decreasing network performance $\varphi(t)$ (adapted from Henry & Ramirez-Marquez (2012))

In this study, the focus is on the recovery period after t_d, for which a model that optimizes a restoration plan over a finite planning horizon is proposed. Without loss of generality, let $t \in \{1 \dots T\}$ denote the time periods over which the CI network is restored and $t = t_d = 0$ denote the instant of planning. The system performance $\varphi(t)$, $t \in \{1 \dots T\}$ is defined using a maximum weighted flow performance metric defined over an undirected network $G(V, E)$ that represents the CI. The nodes V are partitioned into supply nodes V^+, transshipment nodes V^*, and demand nodes such that $V^+ \cup V^* \cup V^- = V$. Each supply node $i \in V^+$ has a supply $P_i^+ \in \mathbb{R}_0^+$ that specifies the maximum amount of flow that may originate at the node within a single time period. Associated with each demand node $j \in V^-$ is a demand $P_j^- \in \mathbb{R}_0^+$ that specifies the maximum amount of flow that may be consumed by the node in one time period. Each edge $\{i, j\} \in E$ has an associated capacity $P_{ij} \in \mathbb{R}_0^+$ that specifies the maximum amount of flow that can be carried on the edge within a single time period.

Given the mechanics expressed above, system performance is defined as the maximum amount of weighted flow consumed by the demand nodes. Let weights $w_j \in \mathbb{Z}^+$ be assigned to each demand node $j \in V^-$. These weights are incorporated in order to enable prioritizing the importance certain types of demand nodes (e.g., it is more important to deliver power to a hospital than to a residential household). Formally, system performance is defined as:

$$\varphi(t) = \sum_{j \in V^-} w_j f_j(t) \tag{1}$$

where $f_j(t)$ is the total flow reaching demand node j in time period $t \in \{1 \dots T\}$.

The proposed restoration planning model aims to reestablish connectivity between supply and demand nodes of a disrupted network by repairing damaged components over a fixed planning horizon. Disruptions are modeled by the removal of a subset of edges, without loss of generality, at time $t = 0$. Hereafter, these edges are referred to as *failed edges*. As edges are repaired in subsequent time periods, the system performance $\varphi(t)$ improves. Following Fang et al. (2016), the resilience $R(T)$ is defined as the cumulative performance restored during the restoration horizon normalized by dividing by the cumulative performance that would be restored over the same horizon if the system could be restored to pre-disruption performance instantaneously. That is, the system resilience is given by:

$$R(T) = \frac{\sum_{t=1}^{t=T} [\sum_{j \in V^-} w_j f_j(t) - \varphi(0)]}{T(\sum_{j \in V^-} w_j P_j^- - \varphi(0))}, \quad T \geq 1 \tag{2}$$

where $\sum_{j \in V^-} w_j P_j^- = \varphi(t_0)$ denotes the system performance if not affected by the disruption.

2.2. Risk measure approach

Generally, two-stage stochastic optimization approaches in the literature are risk-neutral. In other words, these approaches incorporate randomness by comparing different solutions on the basis of expectation. Though solutions to risk-neutral models perform well on average, they may be prone to poor performance for certain realizations in practice. Given the non-repetitive nature of CI restoration and its significant impact on society, it is of interest to consider risk-averse models for planning restoration (Noyan, 2012). That is, a desirable restoration plan may seek to limit the chance of realizations that result in poor performance.

Toward stating a risk-averse restoration optimization model in Section 2.3, we now summarize the Conditional Value at Risk (CVaR) risk measure (Krokhmal et al., 2002; Rockafellar & Uryasev, 2000) and recap results pertinent to the optimization model. Let Z denote a *loss* random variable with cumulative distribution function (CDF) $F(\cdot)$. The term "loss" is used here to indicate that large values of Z are undesirable. Although this convention seemingly conflicts with the "maximize resilience" objective, it has been employed here because it is standard in the CVaR literature. Section 2.3 details the procedure for applying these results to our model.) For a given risk level $\alpha \in [0, 1]$, the Value at Risk (VaR) of Z is defined as:

$$\mathrm{VaR}_\alpha(Z) = \min\{t | F(t) \geq \alpha\} = \min\{t | P(Z \leq t) \geq \alpha\} \tag{3}$$

Thus, for a continuous random variable Z, $\mathrm{VaR}_\alpha[Z]$ is the quantile of Z that exceeds the loss with probability α.

The CVaR for Z with risk level $\alpha \in [0, 1]$ is the expected loss given that the loss is at least $\mathrm{VaR}_\alpha(Z)$, i.e.:

$$\mathrm{CVaR}_\alpha(Z) = \mathbb{E}\left(Z | Z \geq \mathrm{VaR}_\alpha(Z)\right) \tag{4}$$

It is known that CVaR can also be expressed as the optimal solution to the optimization problem:

$$\mathrm{CVaR}_\alpha[Z] = \min_{\eta \in \mathbb{R}} \left\{ \eta + \frac{1}{1-\alpha} \mathbb{E}\left[(Z - \eta)_+\right] \right\} \tag{5}$$

where $(a)_+ := \max(a, 0)$ (Rockafellar & Uryasev, 2000).

Equation (5) enables conveniently formulating risk-averse stochastic optimization models with respect to a CVaR risk measure. Formally, let x be a vector of decision variables, ξ be a random vector of data, and $G(x, \xi)$ be a cost function depending on x and ξ. Then, the CVaR minimization problem:

$$\min_{x \in X} \quad \mathrm{CVaR}_\alpha[G(x, \xi)] \tag{6}$$

can be formulated as:

$$\min_{x \in X, \eta \in \mathbb{R}} \quad \left\{ \eta + \frac{1}{1-\alpha} \mathbb{E}\left[(G(x, \xi) - \eta)_+\right] \right\} \tag{7}$$

allowing us to linearize the model by expressing the expected value term as a probability-weighted

summation of ξ discrete realizations.

2.3. Two-stage stochastic optimization model formulation

This section formulates a two-stage stochastic optimization model in which the first stage schedules the repair of failed edges using multiple repair crews, and the second stage determines the resilience that results under a given realization of the random variables. Rather than optimize explicitly over all random variables, it is common to sample scenarios from their joint distribution. Let Ω denote the set of scenarios. For a given scenario $\omega \in \Omega$, let $ttr_{ij\omega}$ denote the time to repair edge $\{i', j'\} \in E'$ and let $tt_{iji'j'}$ denote the travel time incurred if edge $\{i, j\} \in E'$ and edge $\{i', j'\} \in E'$ are repaired in sequence. It will also be convenient to define $\xi(\omega)$ as a vector specifying the realized values of all random variables in scenario ω.

The maximum weighted flow for each time period $t \in \{1 \dots T\}$ depends on $\xi(\omega)$, and therefore the resilience depends on $\xi(\omega)$ as well. Let $f_{j\omega}(t)$ denote the flow into demand node $j \in V^-$ at time $t \in \{1 \dots T\}$ in scenario $\omega \in \Omega$, and define the resilience $R(T, \xi(\omega))$ in scenario $\omega \in \Omega$ as:

$$R(T, \xi(\omega)) = \frac{\sum_{t=1}^{t=T} [\sum_{j \in V^-} w_j f_{j\omega}(t) - \varphi(0)]}{T(\sum_{j \in V^-} w_j P_j^- - \varphi(0))}, \quad T \geq 1 \tag{8}$$

In what follows, $R(T, \xi(\omega))$ is optimized with respect to both expectation and a CVaR risk measure. For simplicity of exposition, the model for the case of maximizing expected resilience is stated first.

Notation

A summary of notation follows. In addition to the notation already defined, the summary defines binary variables z_{ijk} and $x_{iji'j'k}$ in order to encode a restoration plan, auxiliary binary variables $s_{ij\omega}(t)$ and $y_{ijk\omega}(t)$ in order to resolve the status of each disrupted edge for each time period and realized scenario, and flow variables $f_{ij\omega}(t)$ in order to facilitate determining the maximum weighted flow for each time period and realized scenario. The feasible region of the optimization problem is denoted by X and the sets of decision variables are represented as $\{f,\ s,\ y,\ st,\ z,\ x\}$.

Parameters and sets

$G(V, E)$	Undirected graph consisting of nodes V and edges E
$\{V^+, V^*, V^-\}$	Set of {supply, transshipment, demand} nodes
T	The number of time periods in restoration planning
E'	Set of failed edges before restoration ($E' \subset E$)
K	Set of repair crews
P_i^+	Supply of node $i \in V^+$ per time period
P_j^-	Demand of node $j \in V^-$ per time period
P_{ij}	Flow capacity of edge $\{i, j\} \in E$ per time period
$tt_{iji'j'\omega}$	Travel time between edge $\{i, j\} \in E'$ and $\{i', j'\} \in E'$ in scenario ω
$ttr_{ij\omega}$	Time to repair edge $\{i, j\} \in E'$ for each scenario ω

Decision variables

$f_{ij\omega}(t)$	Flow on edge $\{i, j\} \in E$ in time $t \in \{1 \dots T\}$ for each scenario ω

$f_{j\omega}(t)$	Total flow reaching demand node $j \in V^-$ in each scenario ω
$s_{ij\omega}(t)$	Binary variable indicating whether ($s_{ij\omega} = 1$) or not ($s_{ij\omega} = 0$) edge $\{i,j\} \in E$ is functioning at time $t \in \{0 \dots T\}$
$y_{ijk\omega}(t)$	Binary variable that equals 1 if edge $\{i,j\} \in E'$ is assigned to crew $k \in K$ and it is functioning at time $t \in \{0 \dots T\}$; 0 otherwise
$st_{ijk\omega}$	Time at which crew $k \in K$ begins repairing edge $\{i,j\} \in E'$
z_{ijk}	Binary variable that equals 1 if edge $\{i,j\} \in E'$ is assigned to crew $k \in K$; 0 otherwise
$x_{iji'j'k}$	Binary variable that equals 1 if crew $k \in K$ repairs edge $\{i,j\} \in E'$ before edge $\{i',j'\} \in E' \setminus \{i,j\}$

The two-stage stochastic optimization model for maximizing the expected resilience follows:

$$\max_{\{f,s,y,st,z,x\} \in X} \mathbb{E}(R(T, \xi(\omega))) \tag{9}$$

s.t.

$$\sum_{ij \in E} f_{ij\omega}(t) - \sum_{ji \in E} f_{ji\omega}(t) \ \leq P_i^+, \ \forall i \in V^+, \ \forall t \in \{1 \dots T\}, \ \forall \omega \in \Omega \tag{10}$$

$$\sum_{ij \in E} f_{ij\omega}(t) - \sum_{ji \in E} f_{ji\omega}(t) = 0, \ \forall i \in V^*, \ \forall t \in \{1 \dots T\}, \ \forall \omega \in \Omega \tag{11}$$

$$\sum_{ij \in E} f_{ij\omega}(t) - \sum_{ji \in E} f_{ji\omega}(t) \ = f_{j\omega}(t) \ , \ \forall j \in V^-, \ \forall t \in \{1 \dots T\}, \ \forall \omega \in \Omega \tag{12}$$

$$0 \leq f_{j\omega}(t) \ \leq P_j^-, \ \forall j \in V^-, \ \forall t \in \{1 \dots T\}, \ \forall \omega \in \Omega \tag{13}$$

$$-s_{ij\omega}(t) P_{ij} \leq f_{ij\omega}(t) \ \leq s_{ij\omega}(t) P_{ij}, \ \forall ij \in E, \ \forall t \in \{1 \dots T\}, \ \forall \omega \in \Omega \tag{14}$$

$$s_{ij\omega}(0) = 0, \forall ij \in E', \ \forall \omega \in \Omega \tag{15}$$

$$s_{ij\omega}(0) = 1, \forall ij \in E \backslash E', \ \forall \omega \in \Omega \tag{16}$$

$$s_{ij\omega}(t) \ \leq s_{ij\omega}(t+1) \ , \ \forall ij \in E, \ \forall t \in \{0 \dots T-1\}, \ \forall \omega \in \Omega \tag{17}$$

$$y_{ijk\omega}(t) \ \leq y_{ijk\omega}(t+1) \ , \ \forall ij \in E', \ \forall t \in \{0 \dots T-1\}, \ \forall k \in K, \ \forall \omega \in \Omega \tag{18}$$

$$st_{ijk\omega} + ttr_{ij\omega} + tt_{iji'j'\omega} \leq st_{i'j'k\omega} + M x_{iji'j'k}, \ \forall ij, i'j' \ \in E' \ : \ \{i,j\} \neq \{i',j'\}, \ \forall k \in K, \ \forall \omega \in \Omega \tag{19}$$

$$st_{ijk\omega} + ttr_{ij\omega} + tt_{iji'j'\omega} \leq st_{i'j'k\omega} + M(1 - x_{iji'j'k}), \forall ij, i'j' \ \in E' \ : \ \{i,j\} \neq \{i',j'\}, \ \forall k \in K, \forall \omega \in \Omega \tag{20}$$

$$t \geq st_{ijk\omega} + ttr_{ij\omega} - M[1 - y_{ijk\omega}(t)] \ , \forall ij \in E', \ \forall t \in \{1 \dots T\}, \ \forall k \in K \ , \forall \omega \in \Omega \tag{21}$$

$$\sum_{k \in K} y_{ijk\omega}(t) \ = s_{ij\omega}(t) \ , \forall ij \in E', \ \forall t \in \{0 \dots T\}, \ \forall \omega \in \Omega \tag{22}$$

$$\sum_{\omega \in \Omega} y_{ijk\omega}(t) \ \geq \sum_{\omega \in \Omega} s_{ij\omega}(T) - |\Omega|(1 - z_{ijk}) \ , \forall ij \in E', \ \forall k \in K \tag{23}$$

$$\sum_{\omega \in \Omega} y_{ijk\omega}(t) \ \leq |\Omega| z_{ijk} \ , \forall ij \in E', \ \forall k \in K \tag{24}$$

$$\sum_{k \in K} z_{ijk} \ = 1 \ , \forall ij \in E' \tag{25}$$

$$x_{iji'j'k} \in \{0,1\}, \ \forall ij \in E', \ \forall i'j' \in E' \setminus \{i,j\}, \ \forall k \in K \tag{26}$$

$$z_{ijk} \in \{0,1\}, \ \forall ij \in E', \ \forall k \in K \tag{27}$$

$$y_{ijk\omega}(t) \in \{0,1\}, \ \forall ij \in E', \ \forall t \in \{1 \dots T\}, \forall k \in K, \forall \omega \in \Omega \tag{28}$$

$$s_{ij\omega}(t) \in \{0,1\}, \ \forall ij \in E, \ \forall t \in \{1 \dots T\}, \forall \omega \in \Omega \tag{29}$$

$$st_{ijk\omega} \geq 0,\ \forall ij \in E',\ \forall k \in K,\ \forall \omega \in \Omega \tag{30}$$

The goal of model (9)–(30) is to determine a sequence of edges for each crew to restore in order to maximize the expected resilience. Constraints (10)–(12) are flow balance constraints. Constraint (13) ensures that each demand node $j \in V^-$ consumes no more than its demand P_j^- in every time period, and constraint (14) ensures that the flow on each edge $\{i,j\} \in E$ in each time period does not exceed its capacity P_{ij} if the edge is functioning or 0 if the edge is failed. Constraints (15) and (16) set the initial state of edges to be 0 for failed edges and 1 for other edges. Constraint (17) ensures that edges $\{i,j\} \in E'$ remain functioning after being restored, and edges $\{i,j\}$ are functioning for the entire restoration period. Constraint (18) impose a similar restriction on the $y_{ijk\omega}(t)$-variables; that is, if an edge $\{i,j\} \in E'$ was repaired by crew $k \in K$ by time period $t \in \{1 \dots T-1\}$, where $y_{ijk\omega}(0) = s_{ij\omega}(0)$ at $t = 0$, then the edge was also repaired by crew k by time period $t+1$. Constraints (19)–(20) ensure each crew $k \in K$ can work on repairing at most one edge at a time, according to the schedule specified by the $x_{iji'j'k}$-variables. Note that one limitation of the proposed model is that the $x_{iji'j'k}$ decision variables controlling the schedule of failed components are first-stage decision variables (i.e., not indexed by scenario ω) which prevents sequential changes over time. Relative to Constraints (19)–(20), the $x_{iji'j'k}$-variables, and the $st_{ijk\omega}$-variables, an important detail of the model is that *all* edges are sequenced for repair by *all* crews; however, constraints (14) and (21)–(22) impose that no benefit is gained by (i) completing an edge's restoration after the end of the restoration period or (ii) completing an edge's restoration using a different crew from when it was first restored. Therefore, the effect is equivalent to imposing strictly that each edge is restored at most once and that edges cannot be restored unless they can be completed during the restoration horizon. Defining $ttr_{ij\omega}^{\max}$ and $tt_{iji'j'\omega}^{\max}$ as the maximum repair time parameter of any failed edge in all scenarios and the maximum travel time parameter between any two failed edges in all scenarios, $M = |E'|(ttr_{ij\omega}^{\max} + tt_{iji'j'\omega}^{\max})$ is sufficiently large in Constraints (19)–(20). Constraint (21) ensures that an edge $\{i,j\} \in E'$ cannot have been restored by crew $k \in K$ by time t unless the restoration start time added to the repair time is no more than t. In Constraint (21), it is sufficient to use the same value for M as in constraints (19)–(20). Constraint (22) imposes that an edge $\{i,j\} \in E'$ repaired by crew $k \in K$ by time $t \in \{1 \dots T\}$ is an edge that must be functioning at time t, and it prevents duplicate restoration of an edge by multiple crews. Constraints (26)–(29) require the $x_{iji'j'k}$-, z_{ijk}-, $y_{ijk\omega}(t)$-, and $s_{ij\omega}(t)$ variables to to be binary, and Constraint (30) imposes that no repair tasks begin prior to time $t = 0$.

The risk-neutral model (9)–(30) can be reformulated using a CVaR objective by first introducing the following resilience loss function:

$$\Delta R(T, \xi(\omega)) = 1 - R(T, \xi(\omega)) \tag{31}$$

The value of $\Delta R(T\xi(\omega))$ ranges between $[0,1]$ because $R(T)$ is bounded by the same values. Given that X denotes the feasible region determined by constraints (10)–(30) and $\{f, s, y, st, z, x\}$ represents the set of decision variables, then, by using Equation (7) the CVaR problem can be formulated as:

$$\min_{\{f,\, s,\, y,\, st,\, z,\, x\} \in X,\ \eta \in \mathbb{R}} \quad \left\{ \eta + \frac{1}{1-\alpha} \mathbb{E}\left[(\Delta R(T, \xi(\omega)) - \eta)_+ \right] \right\} \tag{32}$$

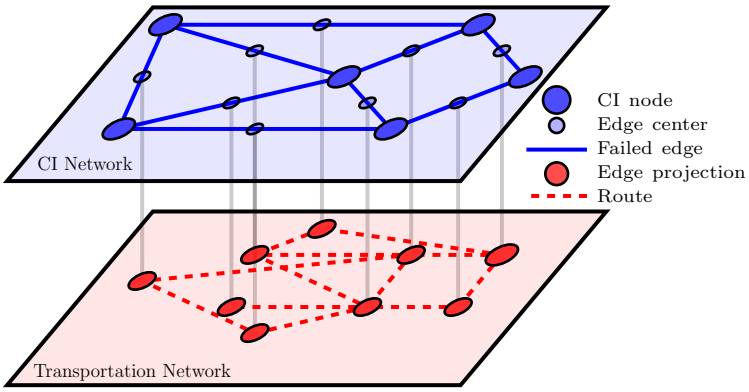

Figure 2: Projection of CI network edges on transportation network

To motivate the following section, consider an optimal solution to model (32). Observe that the CVaR for this solution corresponds to the average resilience loss of the $\lceil (1-\alpha)|\Omega| \rceil$ worst scenarios (having values greater than η); thus, the remaining $\lfloor \alpha|\Omega| \rfloor$ scenarios contribute to the CVaR only indirectly because their resilience loss must be no more than η. Following Arpón et al. (2018) and García-Bertrand & Mínguez (2012), this motivates a computationally efficient strategy for deriving solutions to model (32) by reducing the set of scenarios to focus on those that involve high risk.

3. Solution approach

3.1. Scenario generation and reduction

To ensure a representative set of scenarios, a maxi-min Latin hypercube sampling (LHS) technique (Wyss & Jorgensen, 1998) is used to generate a large set of scenarios Ω. Using LHS ensures some amount of coverage of each random variable's range, and it has been shown to have advantages when incorporated within a sample average approximation approach (Chen et al., 2014; Kleywegt et al., 2002).

When the number of generated scenarios is large, the associated stochastic program tends to become intractable (Morales et al., 2009). To improve tractability, one method is to reduce the number of scenarios such that the resulting problem's optimal solution is close to the solution of the original optimization problem (Fang & Sansavini, 2019). In these methods, which have received significant attention in the literature (Heitsch & Römisch, 2003; Horejšová et al., 2020), it is common to select scenarios based upon a *probability distance* between the original and reduced set of scenarios. The most common probability distance used in stochastic optimization is the Kantorovich distance, $D_K(\cdot)$, defined between two probability distributions Q and Q' on Ω by the following problem (Dupačová et al., 2003; Rachev, 1991):

$$D_K\left(Q, Q'\right) = \inf_{\theta} \left\{ \int_{\Omega\times\Omega} c\left(\omega, \omega'\right) \theta\left(d\omega, d\omega'\right) : \int_{\Omega} \theta\left(\cdot, d\omega'\right) = Q \right. \\ \left. \int_{\Omega} \theta(d\omega, \cdot) = Q' \right\} \tag{33}$$

Problem (33) is known as the Monge–Kantorovich mass transportation problem (Rachev, 1991), where $c\left(\omega, \omega'\right)$ is a nonnegative, continuous and symmetric function, often referred to as cost function. The

infimum is taken over all joint probability distributions defined on $\Omega \times \Omega$ represented by $\theta(\omega, \omega')$ in (33). Note that $D_K(\cdot)$ can only be properly called Kantorovich distance if function $c(\cdot)$ is given by a norm. When Q and Q' are finite distributions corresponding to the initial set of scenarios Ω and the reduced set of scenarios $\Omega_s \subseteq \Omega$, the Kantorovich distance can be determined (see Dupačová et al. (2003) for details) by:

$$D_K(Q, Q') = \sum_{\omega \in \Omega \setminus \Omega_s} \pi_\omega \min_{\omega' \in \Omega_s} c(\omega, \omega') \tag{34}$$

where π_ω represents the probability of scenario ω in Ω (Dupačová et al., 2003). Expression (34) can be used to derive several heuristics for generating reduced scenario sets that are close to an original set (Dupačová et al., 2003; Morales et al., 2009). Practically, the fast forward selection algorithm (Heitsch & Römisch, 2003) has been known to perform well in different stochastic optimization applications. This algorithm is an iterative greedy process that starts with an empty set. In the first step of the algorithm, the scenario that has the minimum probability distance (e.g., Kantorovich distance) with all other scenarios is included. After that, in each step of the algorithm, a scenario that minimizes the Kantorovich distance between the reduced and original sets is selected from the set of non-selected scenarios ($\Omega \setminus \Omega_s$), where Ω_s represents the set of selected scenarios. Then, this scenario is included in the reduced set Ω_s. The stopping criteria of the algorithm is either by finding the pre-specified number of scenarios or by reaching a pre-defined Kantorovich distance threshold (Morales et al., 2009).

In the fast forward selection algorithm, as described in (Heitsch & Römisch, 2003), the distance between two scenarios ω and ω' is expressed by the function $c(\omega, \omega')$ and is computed according to the difference between pairs of random vectors. Choices of the function (distance) $c(\omega, \omega')$ varies between probability metrics (Dupačová et al., 2003), fixed first-stage decision variables objective function (Morales et al., 2009) and the objective value for each scenario, which is shown to practically outperform the other two methods (Bruninx, 2014). Here, we use the objective function value z_ω^{WS} of the *wait-and-see solution* (WS) for each scenario $\omega \in \Omega$ (i.e., the objective function resulting from solving model (9)–(30) when it is populated with ω as its only scenario) to define $c(\cdot, \cdot)$ as follows:

$$c(\omega, \omega') = \left| z_\omega^{WS} - z_{\omega'}^{WS} \right| \tag{35}$$

The resulting fast forward selection algorithm is summarized in Algorithm 1, specifically using the "Algorithm A" subroutine in Step 0. We apply this algorithm, hereafter referred to as "Algorithm 1-A, to the risk-neutral model (9). We also compare Algorithm 1-A to Algorithm 1-B, which is the standard algorithm proposed by Dupačová et al. (2003) based on the difference between the realized vectors $\boldsymbol{\lambda}_\omega$ and $\boldsymbol{\lambda}_{\omega'}$ consisting of the travel times and repair times for a pair of scenarios $\omega, \omega' \in \Omega$:

$$c(\omega, \omega') = \| \boldsymbol{\lambda}_\omega - \boldsymbol{\lambda}_{\omega'} \| \tag{36}$$

and report our findings in Section 4.4.

Following Arpón et al. (2018), Fairbrother et al. (2019) and Pineda & Conejo (2010), Algorithm 1 is adapted to the CVaR model given in Equation (32). Toward this end, we first define an active scenario subset $\Omega_\alpha \subseteq \Omega$ of scenarios consisting of the scenarios $\omega \in \Omega$ having the worst WS objective

value z_{ω}^{WS} (García-Bertrand & Mínguez, 2012). Formally, let $\eta_{\alpha}^{*} = \text{VaR}_{\alpha}[G(x_{\omega}^{*}, \cdot)]$ and define $\Omega_{\alpha} = \{\omega \in \Omega : G(x_{\omega}^{*}, \xi(\omega)) \geq \eta_{\alpha}^{*}\}$.

Algorithm 1-C (i.e., Algorithm 1 with the "Algorithm C" subroutine chosen in Step 0) summarizes the resulting procedure. After performing this initial reduction, Algorithm 1-C proceeds exactly as Algorithm 1-A.

The current risk-averse scenario reduction approach combines the active scenarios concept from García-Bertrand & Mínguez (2012) and the WS reduction metric from Bruninx (2014). One advantage of this hybrid procedure is that the auxiliary variable η in Equation (32) is already known ($\eta = \eta_{\alpha}^{*} = \text{VaR}_{\alpha}[G(x_{\omega}^{*}, \cdot)]$) given that individual scenario problems are already solved and that only scenarios whose resilience losses are greater than or equal to η_{α}^{*} are chosen. This allows us to rewrite Equation (32) with optimal $\text{VaR}_{\alpha}[G(x_{\omega}^{*}, \cdot)]$ as:

$$\min_{\{f,\, s,\, y,\, st,\, z,\, x\} \in X} \quad \left\{ \eta_{\alpha}^{*} + \frac{1}{1-\alpha} \mathbb{E}\left[(\Delta R(T, \xi(\omega)) - \eta_{\alpha}^{*}) \right] \right\} \tag{37}$$

In addition, since the subset of $1 - \alpha$ scenarios in Ω_{α} is treated as a whole set of α- CVaR included scenarios—with each scenario ω included in Ω_{α} having the property of $G(x_{\omega}^{*}, \xi(\omega)) \geq \eta_{\alpha}^{*}$—we can drop the constant η_{α}^{*} and express Equation (37) as:

$$\min_{\{f,\, s,\, y,\, st,\, z,\, x\} \in X} \quad \left\{ \frac{1}{1-\alpha} \mathbb{E}\left[(\Delta R(T, \xi(\omega)) | \omega \in \Omega_{\alpha} \right] \right\} \tag{38}$$

Thus, the problem has become similar to the risk-neutral one by choosing the risk region Ω_{α} and the reduction Algorithm 1-C acts similar to Algorithm 1-A as mentioned above. Nonetheless, the disadvantage of the approach suggested by Pineda & Conejo (2010) and its risk-averse extension proposed in this paper is that the algorithm computational time will be higher than other approaches. To overcome the problem, we provide the deterministic solution (DS) as the initial feasible solution to solve the problem associated with each scenario reducing the computational time significantly to a level on par with Morales et al. (2009).

3.2. Benders decomposition

There are different types of decomposition algorithms for solving continuous and mixed integer large-scale two-stage and multi-stage optimization problems (see Escudero et al. (2017) for a recent review). One of those types of algorithms is the time-honored Benders decomposition (Benders, 1962) and its variants (see Rahmaniani et al. (2017) for a good review). Benders decomposition is commonly used in the stochastic optimization literature to solve the resulting mixed-integer linear programs (Rahmaniani et al., 2017). In this context, the risk-neutral and risk-averse models separate into one linear program per scenario ω—forming what is known as the subproblem (SP)—in the reduced scenario set Ω_s ($\Omega_{\alpha,s}$ for the CVaR model) after fixing the binary $x_{iji'j'k}$-, z_{ijk}-, $y_{ijk\omega}(t)$-, and $s_{ij\omega}(t)$-variables.

Formally, for each scenario $\omega \in \Omega_s$, let $\overline{\boldsymbol{z}}_{\omega}$ denote a fixed assignment of values to all x-, z-, y-, and s-variables corresponding to the index ω. The resulting SP for scenario $\omega \in \Omega_s$—with resilience loss

Algorithm 1: Fast forward scenario reduction algorithm (Dupačová et al., 2003)

Step 0: Compute the distances of scenario pairs:

Algorithm A: $c(\omega,\omega') = \left|z_\omega^{WS} - z_{\omega'}^{WS}\right|;\ \forall\omega,\omega' \in \Omega$ ▷ Risk-neutral WS

Algorithm B: $c(\omega,\omega') = \|\boldsymbol{\lambda}_\omega - \boldsymbol{\lambda}_{\omega'}\|;\ \forall\omega,\omega' \in \Omega$ ▷ $\boldsymbol{\lambda}$ is a vector of random variables

Algorithm C: (a) $\Omega_\alpha = \{\omega \in \Omega \mid G(x_\omega^*,\omega) \geq \eta_\alpha^*\}$ ▷ proposed risk-averse

(b) $c(\omega,\omega') = \left|z_\omega^{WS} - z_{\omega'}^{WS}\right|;\ \forall\omega,\omega' \in \Omega_\alpha$ ▷ $\Omega = \Omega_\alpha$ and $\Omega_s = \Omega_{\alpha,s}$ for Algorithm C in steps 1-3

Step 1: Select the first scenario as the most equidistant scenario from all other scenarios in the set Ω :

$$\omega_1 = \arg\min_{\omega'\in\Omega}\left\{\sum_{\omega\in\Omega}\pi_\omega c(\omega,\omega')\right\} \tag{39}$$

$\Omega_s^{[1]} \leftarrow \{\omega_1\}$ ▷ $\Omega_s^{[i]}$ is the set of selected scenarios until step i

$\Omega_J^{[1]} \leftarrow \Omega\backslash\{\omega_1\}$ ▷ $\Omega_J^{[i]}$: the scenarios set not selected in the first i steps

Step *i*: Identify the scenarios ω_i to be added to Ω_s until it reaches a given cardinality N_s based on the distance function between $\Omega_s^{[i-1]}$ and $\Omega_J^{[i-1]}$:

For i in $\{2\dots N_s\}$:

$$\omega_i = \arg\min_{\omega'\in\Omega_J^{[i-1]}}\left\{\sum_{\omega\in\Omega_J^{[i-1]}\backslash\{\omega'\}}\pi_\omega \min_{\omega''\in\Omega_s^{[i-1]}\cup\{\omega\}} c(\omega,\omega'')\right\} \tag{40}$$

$\Omega_s^{[i]} \leftarrow \Omega_s^{[i-1]} \cup \{\omega_i\}$, $\Omega_J^{[i]} \leftarrow \Omega_J^{[i-1]}\backslash\{\omega_i\}$ ▷ $\Omega_J^{[i]} \cup \Omega_s^{[i]} = \Omega$

End For

Step *N_s+1*: Redistribute the probabilities of $\Omega_J^* = \Omega_J^{[N_s]}$ over $\Omega_s^* = \Omega_s^{[N_s]}$ according to the cost function $c(\omega,\omega')$:

$$\pi_\omega^* = \pi_\omega + \sum_{\omega'\in J(\omega)}\pi_{\omega'},\ \ \forall\omega \in \Omega_s^* \tag{41}$$

with $J(\omega)$ being the set of scenarios $\omega' \in \Omega_J^*$ such that $\omega = \arg\min_{\omega''\in\Omega_s^*} c(\omega'',\omega')$

minimization objective—is the linear program:

$$\mathrm{SP}(\overline{\boldsymbol{z}}_\omega):\quad \min\left(1 - \frac{\sum_{t=1}^{t=T}\left[\sum_{j\in V^-} w_j f_{j\omega}(t) - \varphi(0)\right]}{T\left(\sum_{j\in V^-} w_j P_j^- - \varphi(0)\right)}\right) \tag{42}$$

$$\text{s.t. } (10)-(14) \text{ for scenario } \omega \tag{43}$$

Because $\mathrm{SP}(\overline{\boldsymbol{z}}_\omega)$ is a linear program in which $\overline{\boldsymbol{z}}_\omega$ appears only in the constraints, the dual of $\mathrm{SP}(\overline{\boldsymbol{z}}_\omega)$ can be formulated as a linear program of the form:

$$\mathrm{DSP}(\overline{\boldsymbol{z}}_\omega):\quad \max\quad (\boldsymbol{b} - \boldsymbol{B}\overline{\boldsymbol{z}}_\omega)\,\boldsymbol{d}_\omega \tag{44}$$

$$\text{s.t. } \boldsymbol{d}_\omega \in \mathcal{D} \tag{45}$$

where $\boldsymbol{b}$ is the right-hand side vector of (43), $\boldsymbol{B}$ is the left-hand side coefficient matrix of (43), $\boldsymbol{d}_\omega$ is the dual variable vector corresponding to constraint (43), and $\mathcal{D}$ represents the dual feasible region. Let $\mathcal{D}_p$ and $\mathcal{D}_r$ respectively denote the extreme points and extreme rays of $\mathcal{D}$. Then, letting $\mathcal{D}_p^{\omega n} \subseteq \mathcal{D}_p$ and $\mathcal{D}_r^{\omega n} \subseteq \mathcal{D}_r$ respectively denote a subset of the extreme points and extreme rays produced prior to iteration n of Benders decomposition, the restricted master problem (RMP) for iteration n is

formulated as:

$$\min \quad \sum_{\omega=1}^{\Omega_s} \pi_\omega v_\omega \tag{46}$$

s.t.

$$v_\omega \geq (\boldsymbol{b} - \boldsymbol{B}\boldsymbol{z}_\omega)\, \overline{\boldsymbol{d}}_\omega, \forall \omega \in \Omega_s,\ \overline{\boldsymbol{d}}_\omega \in \mathcal{D}_p^{\omega n} \tag{47}$$

$$0 \geq (\boldsymbol{b} - \boldsymbol{B}\boldsymbol{z}_\omega)\, \overline{\boldsymbol{d}}_\omega, \forall \omega \in \Omega_s,\ \overline{\boldsymbol{d}}_\omega \in \mathcal{D}_r^{\omega n} \tag{48}$$

$$\text{constraints (15)–(30)}$$

where v_ω is a new variable that represents the resilience loss in scenario ω. Constraints (47) and (48) are respectively known as *optimality cuts* and *feasibility cuts*.

In the proposed Benders algorithm (Algorithm 2), the first step is to set the upper bound, lower bound and iteration counter at ∞, 0 and 0, respectively. In iteration n, RMP is solved first to obtain an optimal solution $\bar{\boldsymbol{z}}^n$ (note that in iteration 0, RMP has no cuts and any feasible solution to (15)–(30) is optimal with an objecive value of 0). From $\bar{\boldsymbol{z}}^n$, let $\bar{\boldsymbol{z}}_\omega^n$ denote the partial solution associated with the x-, z-, y-, and s-variables corresponding to the index ω. Then, DSP($\bar{\boldsymbol{z}}_\omega^n$) is solved (note that since the linear program in (42)–(43) and so its dual (44)–(45) are scenario indexed, they can be solved in parallel), yielding either an extreme point $\overline{\boldsymbol{d}}_\omega \in \mathcal{D}_p$ (if the model is solved to optimality) or an extreme ray $\overline{\boldsymbol{d}}_\omega \in \mathcal{D}_p$ (if the model is concluded to be unbounded). In the former case, $\overline{\boldsymbol{d}}_\omega$ is added to $\mathcal{D}_p^{\omega n}$ (i.e., $\mathcal{D}_p^{\omega,n+1} \leftarrow \mathcal{D}_p^{\omega n} \cup \{\overline{\boldsymbol{d}}_\omega\}$ and $\mathcal{D}_r^{\omega,n+1} \leftarrow \mathcal{D}_r^{\omega n}$), resulting in a new optimality cut; otherwise, $\overline{\boldsymbol{d}}_\omega$ is added to $\mathcal{D}_r^{\omega n}$ (i.e., $\mathcal{D}_p^{\omega,n+1} \leftarrow \mathcal{D}_p^{\omega n}$ and $\mathcal{D}_r^{\omega,n+1} \leftarrow \mathcal{D}_r^{\omega n} \cup \{\overline{\boldsymbol{d}}_\omega\}$), yielding a new feasibility cut. The RMP objective provides a lower bound to the optimal solution of the original problem (9)–(30) —under a resilience loss minimization objective—; furthermore, as demonstrated in the following proposition, the dual subproblem DSP($\overline{\boldsymbol{z}}_\omega$) always has an optimal solution, meaning the weighted sum $\sum_{\omega\in\Omega_s} \pi_\omega\, (\boldsymbol{b} - \boldsymbol{B}\overline{\boldsymbol{z}}_\omega^n)\, \overline{\boldsymbol{d}}_\omega$ yields an upper bound. We now state and prove the required result.

Proposition 3.1. *For a given binary variable vector* $\overline{\boldsymbol{z}}_\omega = \left[\overline{x}_{iji'j'k}, \overline{s}_{ij\omega}(t), \overline{y}_{ijk\omega}(t), \overline{z}_{ijk}\right]$ *that satisfies the constraints* (15)–(30)*, both SP*($\overline{\boldsymbol{z}}_\omega$) *and DSP*($\overline{\boldsymbol{z}}_\omega$) *are always feasible and bounded.*

Proof. Observe that setting $f_{ij\omega}(t) = 0,\ \forall \{i,j\} \in E,\ \forall t \in \{1 \dots T\}$, and $f_{j\omega}(t) = 0,\ \forall j \in V^+,\ \forall t \in \{1 \dots T\}$, satisfies Constraints (10)–(14); thus, SP($\overline{\boldsymbol{z}}_\omega$) is feasible. To show the boundedness of SP($\overline{\boldsymbol{z}}_\omega$), note that $f_{j\omega}(t) \leq P_j^-,\ \forall j \in V^-,\ \forall t \in \{1 \dots T\}$ due to Constraint (13); therefore, the objective of SP($\overline{\boldsymbol{z}}_\omega$) is bounded to be nonnegative. By duality theory, DSP($\overline{\boldsymbol{z}}_\omega$) must be feasible and bounded because SP($\overline{\boldsymbol{z}}_\omega$) is feasible and bounded.

This result additionally shows that feasibility cuts are not needed in the decomposition procedure; therefore, only optimality cuts are generated and added to the RMP in each iteration, and the convergence of the algorithm is accelerated.

4. Numerical studies

4.1. System description

To test the proposed model and solution approach, the data from the French electrical power network company RTE (D'Electricité, 2019) is utilized in this work. The RTE network can be modeled

Algorithm 2: Benders decomposition algorithm

Step 0: $UB \leftarrow \infty, LB \leftarrow 0$, iteration counter $n = 0$

Step 1: Solve the RMP to obtain its optimal solution $(\overline{\boldsymbol{z}}_\omega, \bar{v}_\omega), \forall \omega \in \Omega_s$ ▷ $\Omega_s = \Omega_{\alpha,s}$ for CVaR model

$LB \leftarrow \max\{LB, \sum_{\omega \in \Omega_s} \pi_\omega \bar{v}_\omega\}$

Step 2: **For** each $\omega \in \Omega_s$:

Solve the DSP$(\overline{\boldsymbol{z}}_\omega)$ to obtain its optimal solution $\overline{\boldsymbol{d}}_\omega$ and objective value $(\boldsymbol{b} - \boldsymbol{B}\overline{\boldsymbol{z}}_\omega)\,\overline{\boldsymbol{d}}_\omega$

End For

$UB \leftarrow \min\{UB, \sum_{\omega \in \Omega_s} \pi_\omega\,(\boldsymbol{b} - \boldsymbol{B}\overline{\boldsymbol{z}}_\omega)\,\overline{\boldsymbol{d}}_\omega\}$

Step 3: **If** $UB - LB \leq \epsilon$: ▷ ϵ is a predefined tolerance

Stop and report the solution

Else:

(a) Add a total number of $|\Omega_s|$ Benders optimality cuts of the form: $v_\omega \geq (\boldsymbol{b} - \boldsymbol{B}\boldsymbol{z}_\omega)\,\overline{\boldsymbol{d}}_\omega, \forall \omega \in \Omega_s$ to the RMP

(b) $n \leftarrow n + 1$ and go to Step 1

End If

as an undirected graph with 172 substations (nodes) and 220 transmission lines (edges) covering up to more than 17,500 miles. There are 26 power generators and 145 distributors in the network. Some of the generators and distributors also transmit power from other generators to distributors. The weights of the edges (i.e., their capacities) are assumed to be identical. Specially, the capacity of each transmission line is 5000 MW, and the total network flow received by demand nodes is 61928 MW. In addition, given that the power network flow does not follow the general flow-based model introduced in this paper (Bienstock & Mattia, 2007), the DC model has been used as a linear approximation of the power flow in the network (see Appendix A.1 for details).

In this study, three possible cases are considered (along with subcases for their travel times) for network failure modes that differ in terms of their spatial coverage and the importance or criticality of the components in the network:

- **Case 1: Random failures -** common failures that occur randomly across the network caused often by weather-related triggers, man-made accidents and operation errors affecting the whole network. In this case, network edges are removed randomly with an equal failure probability for all edges in the network.

- **Case 2: Cascading failures -** failures of initial components that may cause other interconnected components to fail due to increased loads causing a sequence of failures in the network. The cascading failure process was simulated using the ML model (Motter & Lai, 2002).

- **Case 3: Spatial failures -** failures caused generally by natural disasters (e.g., earthquakes and floods) where only a local spatial area of the network is affected, and thus only components that are spatially close to each other are impacted by the local disruption.

For all these cases, the three subcases of travel times are: (a) without travel time consideration, (b) with deterministic travel time consideration, and (c) with random travel time consideration. Considering these allows for measuring the impact of travel times, uncertainty and risk to be tested under various scenarios of failure propagation and revealing under which circumstances the usage of these

additions to system resilience is critical. The distribution of the failed components over the geographic area of the network for each case can be found in Appendix B.1.

4.2. Uncertainty representation

The proposed model assumes the time to repair each edge and the travel time between failed edges are uncertain, but the remaining parameters are deterministic. The remainder of this section summarizes the assumed probability distributions for the uncertain parameters.

Let $E' \subseteq E$ denote the set of disrupted edges, and ttr_{ij} denote the time to repair edge $e = \{i, j\} \in E'$. We assume $ttr_{i,j}$ has a Weibull distribution with scale parameter ν_e and shape parameter β_e. Specially, the probability density function of ttr_{ij} is given by:

$$h(t, \beta_e, \nu_e) = \frac{\beta_e}{\nu_e} \left(\frac{t}{\nu_e} \right)^{\beta_e - 1} e^{-\left(\frac{t}{\nu_e}\right)^{\beta_e}}, \; t \geq 0 \tag{49}$$

Note that the Weibull distribution is commonly used to model activity times (Abdelkader, 2004).

For $e = \{i, j\} \in E'$ and $e' = \{i', j'\} \in E'$, let $tt_{iji'j'}$ denote the travel time between edge e and e'. A deterministic estimate of the travel time from e to e' is derived using a separate transportation network. In the transportation network, each edge has an associated length and speed limit, and its traversal time c_l is estimated assuming it will always be possible to travel at the speed limit. The deterministic estimate of $tt_{iji'j'}$, hereafter denoted as $dtt_{iji'j'}$, is obtained by determining the shortest path length between two nodes in the transportation network, namely those that are closest to the midpoint of e and e' (see Figure 2 for illustration). To represent the uncertainty of $tt_{iji'j'}$, a distribution for traversal time of edges in the transportation network is populated; given c_l, the random traversal time cr_l is distributed according to the probability mass function:

$$P(cr_l = t) = \begin{cases} 0.3, & t = c_l \\ 0.3, & t = 1.5 \; c_l \\ 0.4, & t = 2 \; c_l \end{cases} \tag{50}$$

and $tt_{iji'j'}$ is found by solving the shortest path problem as explained. This approach follows other disaster relief studies assuming that uncertain traversal times are based on a coefficient multiplication of the deterministic traversal times of the transportation network (de la Torre et al., 2012; Mete & Zabinsky, 2010).

4.3. Assumptions and computational information

In this study, the Weibull distributed repair time shape and scale parameters are assumed to be 5 and 2, respectively, for all components. Such assumptions are made following other studies in the literature in terms of the chosen probability distribution and parameters (Fang & Sansavini, 2019). Thus, the mean-time-to-repair (MTTR) used in the deterministic model is 1.84 hours. Without loss of generality, we assume that 10% of the edges are damaged under each failure mode and that the number of available maintenance crews is three. Table 1 shows the decrease in the network performance under each failure mode. In addition, the restoration planning horizon T is chosen as 20 hours, which is sufficient to restore the network performance to its original state under all cases. For the scenario generation process, 1000 scenarios are generated of each failure mode and its included subcases. After

that, scenario reduction algorithms (Algorithms 1-A and 1-C) were used to reduce the number of scenarios into a smaller set. For the risk-neutral stochastic optimization model, the total number of scenarios is reduced to 10 scenarios; and for the risk-averse stochastic optimization model (with $\alpha = 80\%$) we reduce the total number of scenarios to 5 given that less probability space is covered (80% less) with the CVaR measure. Solutions to the MILPs used in the scenario reduction procedure and the stochastic optimization models were computed using CPLEX 12.10 (CPLEX, 2020) and programmed using Python 3.7 (Python, 2020) on a 3.2 GHz Intel Core i5 iMac machine with 24 GB of RAM.

Case	Random failures	Cascading failures	Spatial failures
Performance drop	9%	13.35%	12.78%

Table 1: Network performance drop after possible modes of disruption

Based on our preliminary analysis, a time limit of 2 hours (7200 seconds) and 1 hour (3600 seconds) was set for each instance of the risk-neutral stochastic optimization model with 10 scenarios and the risk-averse stochastic optimization model with 5 scenarios, respectively. This amount of time allows our implementation of Benders algorithm to solve both problems within 2% adjusted optimality gap (see Appendix A.2 for details) for all subcases. Algorithm 2 was implemented using callbacks with Benders cuts added as lazy constraints. Table 2 shows the added value of our proposed solution algorithm compared to CPLEX standard solver, and Table 3 summarizes the dimensions of different problem instances.

Case	CPLEX standard solver			Benders decomposition		
	Computational time (s)	Gap(%)	Resilience objective value	Computational time (s)	Gap(%)	Resilience objective value
Random failures	7201.05	5.59	0.3437980	7202.178	0.1444	**0.913716**
Random failures (deterministic travel times)	7201.36	5.99	0.3035116	7200.977	0.7702	**0.844289**
Random failures (random travel times)	7201.18	2.56	0.63019	7200.49	0.7646	**0.82157**
Cascading failures	7200.20	1.13	0.8678093	5300.619	1.0288	**0.875282**
Cascading failures (deterministic travel times)	7201.46	2.26	0.78629732	6000.816	0.9407	**0.881616**
Cascading failures (random travel times)	7200.40	6.52	0.481307	7201.611	1.1633	**0.850502**
Spatial failures	7201.83	4.08	0.6243989	7201.101	1.2052	**0.835887**
Spatial failures (deterministic travel times)	7201.15	4.01	0.6289536	7201.170	1.4432	**0.817396**
Spatial failures (random travel times)	7206.79	6.82	0.41048	7217.37	1.3527	**0.800491**

Table 2: Comparison of Benders decomposition and CPLEX solver solutions for the Risk-neutral stochastic optimization model with 10 reduced scenarios

Instance	No. of continuous variables	No. of binary variables	No. of constraints	No. of Scenarios	No. of maintenance crews	Max computational time (s)
Risk-neutral	115,320	315,612	377,104	10	3	7200
Risk-averse	57,660	158,532	188,629	5	3	3600
Deterministic	11,532	32,868	37,695	1	3	600

Table 3: Problem sizes of different study instances

4.4. Results

4.4.1. Scenario reduction results

In this section, we compare the results from the adopted risk-neutral scenario reduction algorithm based on the individual WS solutions with the ones from the standard algorithm based on the norm of

the difference between pairs of scenarios' random vectors. Figure 3 presents a histogram comparison of the WS resilience values of the reduced set of scenarios using the WS metric (Algorithm 1-A) and the standard probability metric (Algorithm 1-B) for one failure mode. The WS reduced scenarios

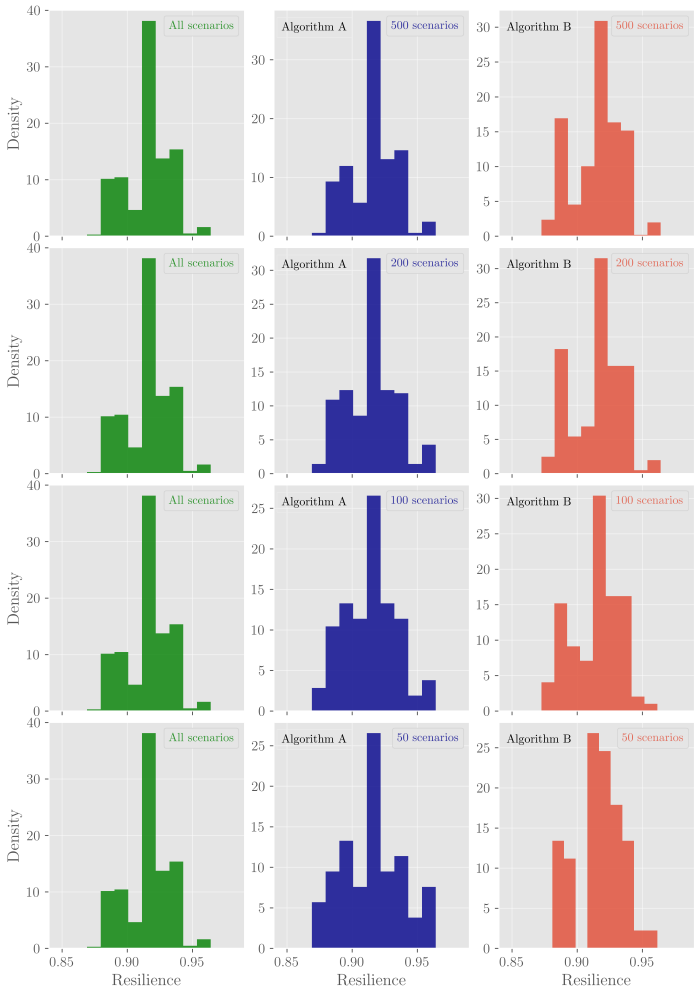

Figure 3: WS results of scenario reduction algorithms 1-A and 1-B for different reduced numbers of scenarios

show more resemblance to the original set of scenarios with respect to the distribution of objective values. Furthermore, Tables 4 and 5 present the values of mean and standard deviation of system resilience for the reduced sets using both algorithms under different target numbers of reduced scenarios without/with travel time considerations. It is worth pointing out that the standard probability metric method cannot differentiate between the model with no travel times and the one considering deterministic travel times since the same set of scenarios will be chosen for both cases.

All 1000 scenarios		Algorithm 1-A			Algorithm 1-B		
Resilience mean	Resilience standard deviation	Number of reduced scenarios	Resilience mean	Resilience standard deviation	Number of reduced scenarios	Resilience mean	Resilience standard deviation
0.915831	0.0172952	500	0.915831	0.0172866	500	0.915613	0.0176127
		200	0.915831	0.0172866	200	0.91598	0.0178898
		100	0.915831	0.0172866	100	0.915249	0.0180558
		50	0.915827	0.0172921	50	0.917131	0.0178635

Table 4: WS results from scenario reduction algorithms 1-A and 1-B for different reduced numbers of scenarios without travel time consideration

All 1000 scenarios		Algorithm 1-A			Algorithm 1-B		
Resilience mean	Resilience standard deviation	Number of reduced scenarios	Resilience mean	Resilience standard deviation	Number of reduced scenarios	Resilience mean	Resilience standard deviation
0.854238	0.0171757	500	0.854238	0.0171671	500	0.853971	0.0174006
		200	0.854238	0.0171671	200	0.854054	0.0177003
		100	0.854239	0.0171649	100	0.853737	0.017949
		50	0.854242	0.0171685	50	0.855148	0.0178526

Table 5: WS results from scenario reduction algorithms 1-A and 1-B for different reduced numbers of scenarios considering deterministic travel times

Table 6 shows the benefit of using a warm start setting (supplying the deterministic solution as an initial feasible solution) for each single scenario problem in reducing both computational time and optimality gaps for the WS problems.

Instance	Average optimality gap (%)	Max optimality gap (%)	Average computational time per problem (s)	Max computational time per problem (s)
1000 scenario with cold start	0.573	2.27	118.135	120
1000 scenario with warm start	0.13	0.59	108.82	120

Table 6: Comparison of computational time and optimality gap for single scenario problems with warm vs. cold start

4.4.2. Stochastic optimization models results

A key result in this study is the impact of the inclusion of travel times between failed components for each maintenance crew on the system resilience. Figure 4 shows a comparison between resilience with and without deterministic travel times for all three failure modes. (The travel time between each pair of failed components is assumed to be $dtt_{iji'j'}$ for the former and 0 for the latter). For all failure modes, the impact of travel times is significant. The result indicates that the resilience models without considering travel times between failed components might overestimate the actual possible resilience values achieved and the time to restore the system to its undisrupted performance. Note that this occurs even in the spatial failures case in which pairs of failed components are likely to be close to each other. A sample of optimal routing for one failure mode is provided in Appendix B.2.

Risk-neutral stochastic model

To measure the added value of incorporating uncertainty into the model and to compare the stochastic solution (SS) to its deterministic counterpart, we use what is known as the value of stochastic solution (VSS) as our metric for comparison. This measure indicates the difference in the objective

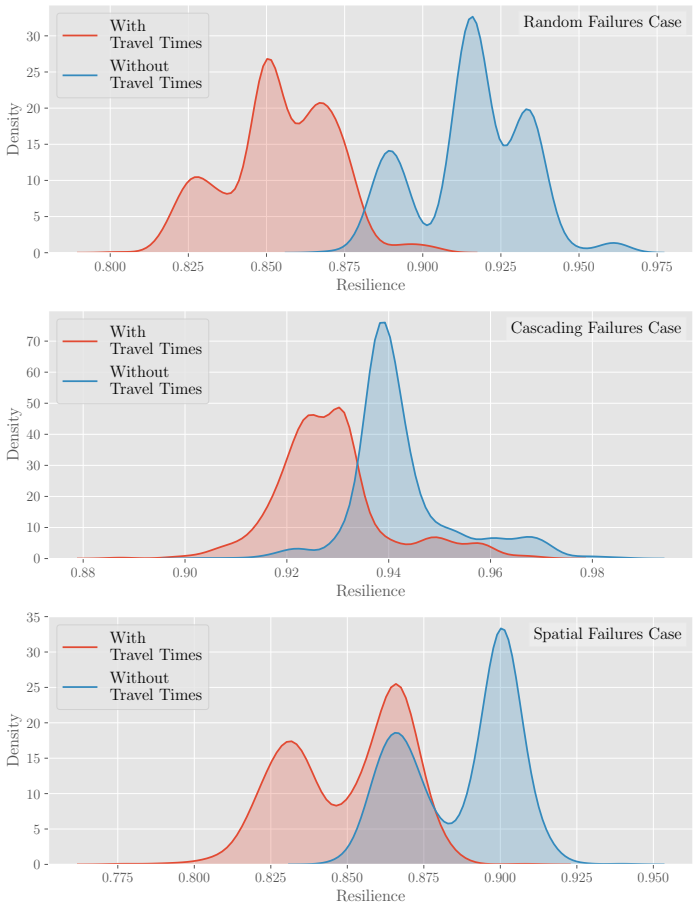

Figure 4: Comparison of resilience values for the 1000 scenarios WSs with/without deterministic travel times

values of the stochastic solution and the deterministic counterpart (Birge, 1982). By solving the restoration problems for the different disruption cases (with the subcases of excluding travel times, and including deterministic travel times and random travel times) using the proposed Benders decomposition method, we can find the added value of uncertainty. Figure 5 shows the added value of the risk-neutral stochastic model compared to its deterministic counterpart in terms of the value of resilience achieved at the end of the restoration period and in terms of the extra amount of flow (power) received by demand nodes under the cases of random failures and cascading failures. Based on that, if the stochastic solution was used instead of the deterministic one, more flow will be pushed to satisfy more demand by amounts of at least 3000 MWh (3 GWh) for all subcases of the random failures case and 1800 MWh (1.8 GWh) for all subcases of the cascading failures case. Given that the annual electricity consumption per household in France is about 5.425 MWh (Odyssee-Mure, 2020) and the daily consumption is approximately 0.015 MWh, the extra amount of flow gained by the stochastic solution is equivalent to the daily consumption of 200,000–275,000 households for case 1 and 100,000–600,000 households for case 2 (see Figure 6). This indicates the significance of incorporating uncertainty into the restoration scheduling tasks.

In contrast to the previous cases, the stochastic solution for the case with spatial failures only

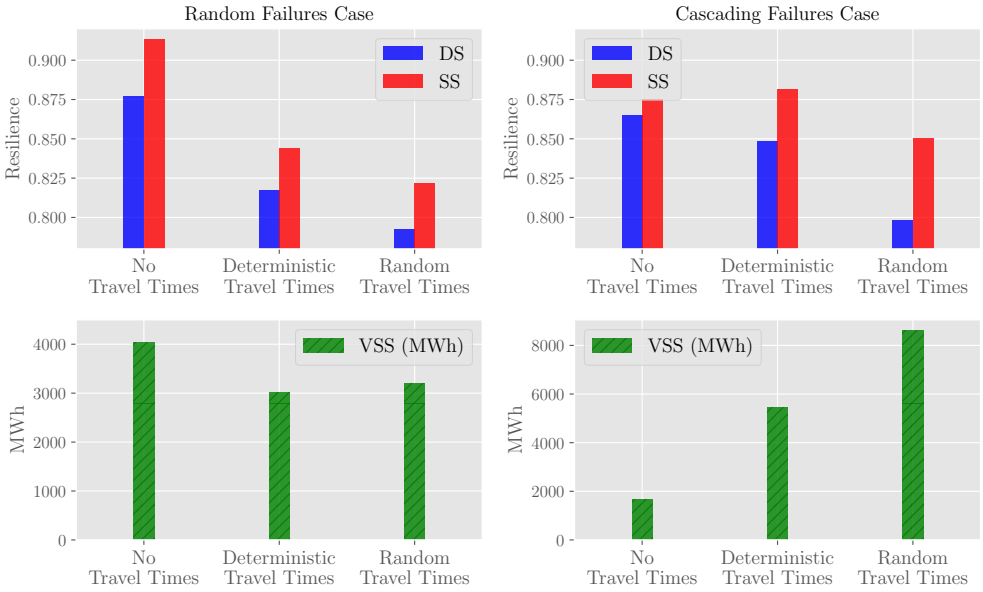

Figure 5: Cases 1 and 2 (Random Failures and Cascading Failures): Resilience values and VSS (as higher satisfied demand in MWh) under different travel time assumptions

shows an improvement over the deterministic solution in the subcase with random travel times. In the other subcases, the deterministic and stochastic solutions are the same. Resilience progress over time curves for cases 1 and 2 can be found under Appendix B.3 showing how the stochastic solution outperforms the deterministic counterpart in almost every scenario.

To validate the solution resulting from the reduced set of scenarios, we compare the solution for each subcase to the one for the full set of scenarios as shown in Table 7. In all subcases, the estimate of the expected resilience value for the small set of scenarios is within about a 0.01 difference from the expected resilience for the full set of scenarios.

Case	Full set of scenarios (1000 scenarios)	Reduced set of scenarios (10 scenarios)
	Resilience objective value	Resilience objective value
Random failures	0.912227	0.913716
Random failures (deterministic travel times)	0.838694	0.844289
Random failures (random travel times)	0.828919	0.82157
Cascading failures	0.881547	0.875282
Cascading failures (deterministic travel times)	0.881711	0.881616
Cascading failures (random travel times)	0.845592	0.850502
Spatial failures	0.848444	0.835887
Spatial failures (deterministic travel times)	0.815873	0.817396
Spatial failures (random travel times)	0.796081	0.800491

Table 7: Validation of solutions for the reduced set of scenarios when applied to the full set of scenarios

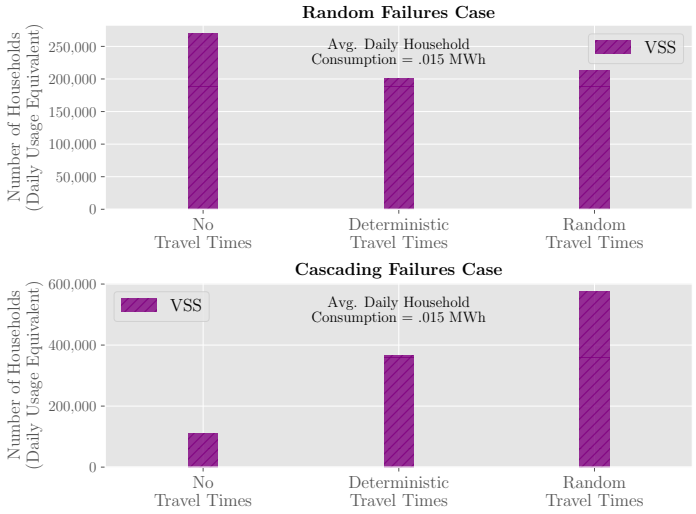

Figure 6: Cases 1 and 2 (Random Failures and Cascading Failures): VSS in equivalent number of households consumption related to the extra amount of satisfied demand in MWh under different travel time assumptions

Risk-averse stochastic model

For the risk-averse model, five reduced scenarios are chosen to represent the worst 20% cases with $\alpha = 0.8$. Similar to the VSS, we adopt the mean-risk value of stochastic solution (MRVSS) (Noyan, 2012), a measure of the possible gain from solving stochastic models incorporating a mean-risk function, as the method to quantify the gains from solving the CVaR problem. However, given that only a CVaR approach is considered rather than a mean-risk one, we rename the measure to CVaR-VSS, i.e., the mean-risk measure with the weight of the expected resilience of scenarios not in α-CVaR being 0. Figures 7, 8 and 9 compare the CVaR solution and the deterministic solution in terms of resilience values and CVaR-VSS for all cases.

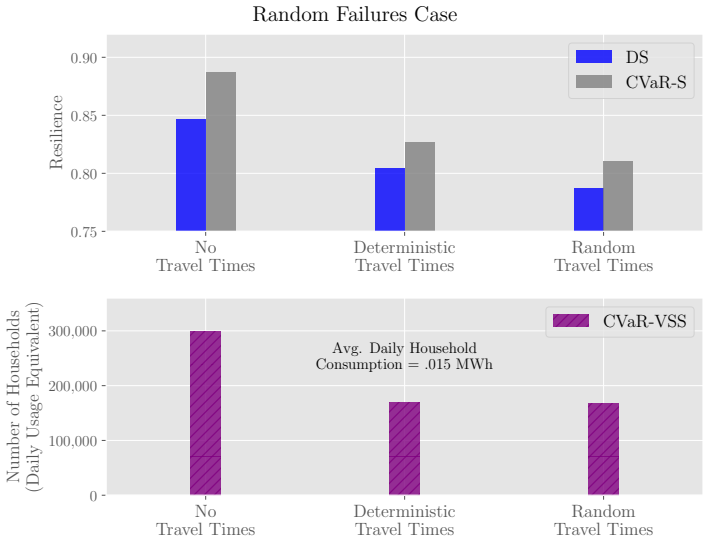

Figure 7: Case 1 (Random Failures): Resilience values and CVaR-VSS in equivalent number of households consumption related to the extra amount of satisfied demand in MWh under different travel time assumptions ($\alpha = 0.8$)

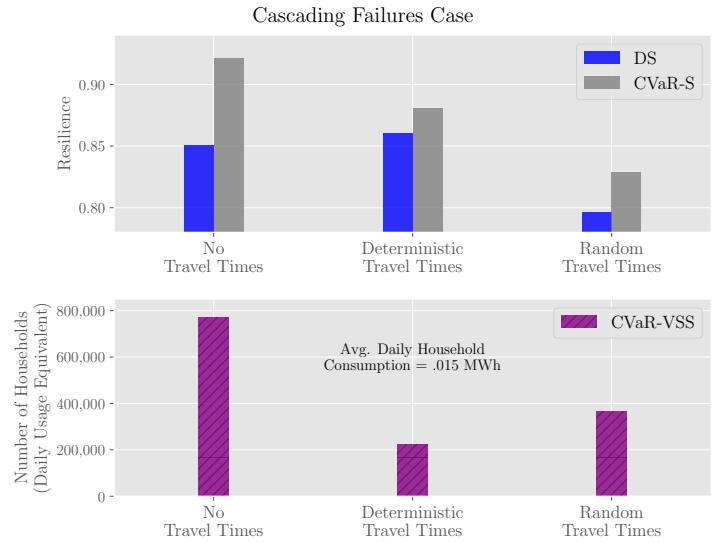

Figure 8: Case 2 (Cascading Failures): Resilience values and CVaR-VSS in equivalent number of households consumption related to the extra amount of satisfied demand in MWh under different travel time assumptions ($\alpha = 0.8$)

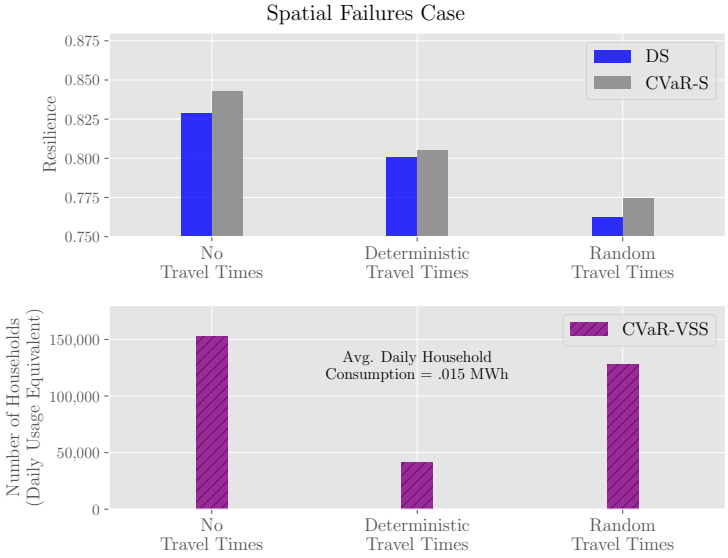

Figure 9: Case 3 (Spatial Failures): Resilience values and CVaR-VSS in equivalent number of households consumption related to the extra amount of satisfied demand in MWh under different travel time assumptions ($\alpha = 0.8$)

In almost all of these cases, the CVaR solutions outperform the deterministic solutions by achieving higher resilience values accompanied with significant CVaR-VSS values ranging from about 50,000 to 800,000 households daily consumption equivalence in the worst-case scenarios. Note that, in contrast to the risk-neutral case, the case with spatial failures also shows a significant CVaR-VSS under all subcases. Figure 10 plots the network performance over time for the high-risk scenarios in Case 3-b (spatial failures with deterministic travel times), showing how the CVaR restoration plan generally achieves full performance in these scenarios faster than either a risk-neutral or deterministic restoration plan.

Table 8 compares the CVaR solution and the deterministic and risk-neutral solutions across Cases 1–3. It can be seen that the risk-averse solution performs the best in all the cases by mitigating the risk associated with resilience loss. Moreover, the risk-neutral solution almost always comes second in performance with the deterministic solution classified as the solution involving the highest risk.

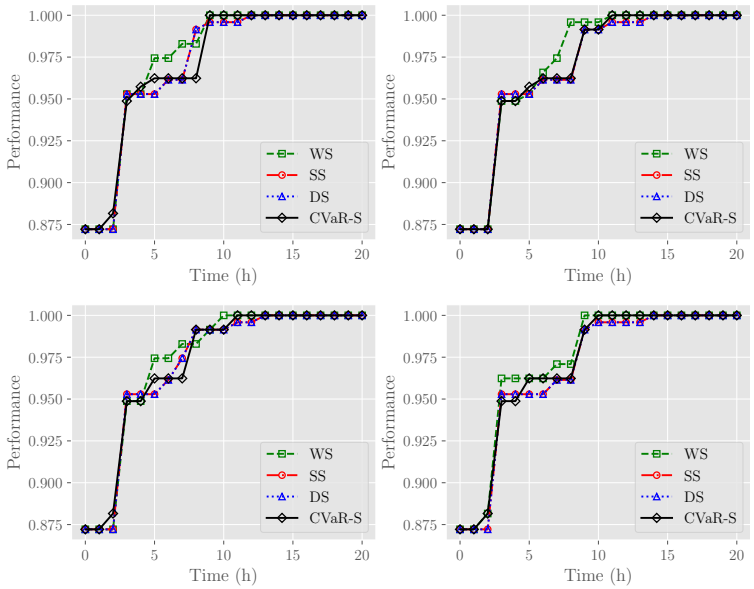

Figure 10: Case 3-b (Spatial Failures with Deterministic Travel Times): Comparison of network performance during the restoration period in high-risk scenarios under different solution plans

In addition, It is of interest to investigate whether the CVaR solution performs well in scenarios other than the high-risk ones. Table 9 compares the risk-neutral solution for all cases with the deterministic counterpart and the CVaR solution applied to the reduced set of 10 scenarios associated with the risk-neutral problem. Surprisingly, the CVaR solution in some cases outperforms the risk-neutral solution. One possible reason of this unexpected finding is that the CVaR problems generally use fewer scenarios, given the $1-\alpha\%$ reduced covered area of possible scenarios allowing the optimal solutions of the problems to be closer to the 0% optimality gap in less amount of computational time. Therefore, two important features of the CVaR approach can be summarized as follows: (1) the CVaR approach covers a fair amount of uncertainty (depending on α value), making its suggested plan more pleasing than the fixed deterministic counterpart, and (2) the CVaR problem is solved with fewer scenarios than its risk-neutral counterpart allowing the optimal solution to be found in less time (50% in our setting) and with lower optimality gaps.

Case	Computational time (s)	Gap(%)	CVaR solution	Deterministic solution	Stochastic solution
Random failures	3600.000	0.0691	**0.887089**	0.846803	0.885704
Random failures (deterministic travel times)	3600.797	0.5549	**0.827217**	0.804466	**0.827217**
Random failures (random travel times)	3600.632	0.833	**0.8103**	0.7876	**0.8103**
Cascading failures	3607.194	0.1988	**0.920725**	0.850712	0.868874
Cascading failures (deterministic travel times)	3600.476	0.8428	**0.880710**	0.860402	0.873507
Cascading failures (random travel times)	3600.035	1.4551	**0.8289**	0.7959	0.8155
Spatial failures	3600.312	0.7766	**0.842965**	0.828520	0.828520
Spatial failures (deterministic travel times)	3600.015	1.4309	**0.804756**	0.800828	0.800828
Spatial failures (random travel times)	3600.896	1.3141	**0.7744**	0.7622	**0.7744**

Table 8: Solution comparison of the risk-averse resilience values ($\alpha = 0.8$) with deterministic and risk-neutral alternatives

Case	Computational time (s)	Gap(%)	Stochastic solution	Deterministic solution	CVaR solution
Random failures	7202.178	0.1444	**0.913716**	0.877421	0.912732
Random failures (deterministic travel times)	7200.977	0.7702	**0.844289**	0.817283	**0.844289**
Random failures (random travel times)	7200.49	0.7646	**0.82157**	0.7928	**0.82157**
Cascading failures	5300.619	1.0288	0.875282	0.865170	**0.911292**
Cascading failures (deterministic travel times)	6000.816	0.9407	0.881616	0.848590	**0.882013**
Cascading failures (random travel times)	7200.4	0.9549	**0.8505**	0.7983	0.8314
Spatial failures	7201.101	1.2052	0.835887	0.835887	**0.850345**
Spatial failures (deterministic travel times)	7201.170	1.4432	0.817396	0.817396	**0.818078**
Spatial failures (random travel times)	7217.37	1.3527	**0.800491**	0.7704	**0.800491**

Table 9: Solution comparison of the risk-neutral resilience values with deterministic and risk-neutral alternatives

5. Conclusion and future work

This paper proposes risk-neutral and risk-averse two-stage stochastic optimization models for CI restoration planning, where post-disruption restoration tasks occur in a highly dynamic environment and thus subject to a considerable amount of uncertainty. The models address two important challenges facing restoration planning, which are the accessibility of failed components and uncertainty associated with restoration task durations and possible starting times. For the former, travel time between components has been added to the model to connect CI restoration models to the state of the underlying transportation network. For the latter, the uncertainty of repair times and travel times is handled by sampling from their suggested probability distributions through a maxi-min Latin hypercube technique, with the number of discrete uncertainty scenarios being reduced to a tractable size by applying an improved risk-neutral and a proposed risk-averse fast forward selection algorithm based on the WS objective values of individual scenarios. The objective of the model is to minimize the expected loss of performance over all possible realizations of the random parameters, and thus to maximize the system's resilience. Three common network failure mechanisms (i.e., random failures, cascading failures and spatial failures) are tested.

The proposed approach was demonstrated using a real-life case study based on the RTE 400 kV French electric power transmission network. Our first finding was the significant impact of incorporating travel times into resilience modeling. In fact, one can see that resilience models that do not consider travel times are overestimating their expected resilience achieved and the speed of restoring the system to its undisrupted performance level. Furthermore, to assess the added value of incorporating uncertainty, two measures were used to quantify the significance of adapting stochastic models over deterministic counterparts: VSS for the risk-neutral stochastic model and CVaR-VSS for the risk-averse stochastic model. Both models have resulted in positive values of VSS and CVaR-VSS in 2 out of 3 cases and all three cases, respectively. There is a clear benefit of using stochastic methods that account for uncertainty over deterministic ones that depend on the expected values of the uncertain parameters. In addition, CVaR solutions were generally found with less computational time, and their suggested restoration plans perform on par with the risk-neutral counterparts and sometimes even better under a risk-neutral setting of scenarios selection. However, under high-risk scenarios, CVaR proposed solutions mitigate the risk associated with such scenarios by achieving resilience values close to the wait-and-see solutions of such individual scenarios. In addition, the CVaR solution under this setting performed second to none under all failure modes and their subcases.

The stochastic optimization models proposed in this study are reformulated as deterministic equivalent large MILPs in order to generate methods to solve proposed models efficiently. A Benders de-

composition algorithm is proposed in this paper to solve the proposed models in short time settings. In addition, given that the risk-averse stochastic program is modeled by a scenario selection procedure identifying true risks associated with individual scenarios, the Benders decomposition algorithm proposed here is robust to work with both versions of the stochastic model. Thus, a practical framework for solving risk-averse versions of resilience-based optimization models, starting from scenarios generation, risk-averse scenarios reduction and ending with a solution procedure, is shown here to facilitate linking risk measures to current and future resilience optimization models.

The proposed stochastic optimization models present a practical framework for risk-neutral and risk-averse resilience-based applications and possibly other applications with task-scheduling procedures involving fair amount of uncertainty. Nonetheless, possible additions in terms of planning flexibility to the current framework are adding multi-mode repairs of failed components and allowing for multi-crew restoration of failed components under travel time considerations. Moreover, restoration considering multiple interdependent networks (Gomez et al., 2019) under uncertainty and network-based risk measures along with coordinating the restoration of the transportation network can also be studied as future research directions. Finally, the models in the present study assume that the restoration plan is determined initially and cannot be altered afterwards. Indeed, relaxing this assumption by enabling sequential change of the plan as time goes on will add more flexibility to the models but will significantly increase the computational time by moving the models from the two-stage setting into a more dynamic multi-stage stochastic optimization framework. Such computational differences can be tested using time-consistent risk-averse measures such as Expected CVaR (Homem-de-Mello & Pagnoncelli, 2016) and Expected Conditional Stochastic Dominance (Escudero et al., 2017).

Acknowledgments

This work was supported by the U.S. National Science Foundation under Grant No. CMMI–1745353.

References

Abdelkader, Y. H. (2004). Evaluating project completion times when activity times are Weibull distributed. *European Journal of Operational Research*, *157*, 704–715.

Aksu, D. T., & Ozdamar, L. (2014). A mathematical model for post-disaster road restoration: Enabling accessibility and evacuation. *Transportation Research Part E: Logistics and Transportation Review*, *61*, 56–67.

Almoghathawi, Y., Barker, K., & Albert, L. A. (2019). Resilience-driven restoration model for interdependent infrastructure networks. *Reliability Engineering and System Safety*, *185*, 12–23.

Anaya-Arenas, A. M., Renaud, J., & Ruiz, A. (2014). Relief distribution networks: a systematic review. *Annals of Operations Research*, *223*, 53–79.

Arpón, S., Homem-de-Mello, T., & Pagnoncelli, B. (2018). Scenario reduction for stochastic programs with conditional value-at-risk. *Mathematical Programming*, *170*, 327–356.

Barker, K., Lambert, J. H., Zobel, C. W., Tapia, A. H., Ramirez-Marquez, J. E., Albert, L., Nicholson, C. D., & Caragea, C. (2017). Defining resilience analytics for interdependent cyber-physical-social networks. *Sustainable and Resilient Infrastructure*, *2*, 59–67.

Benders, J. F. (1962). Partitioning procedures for solving mixed-variables programming problems. *Numerische Mathematik*, *4*, 238–252.

Bienstock, D., & Grebla, G. (2015). Robust control of cascading power grid failures using stochastic approximation. arXiv:1504.00856.

Bienstock, D., & Mattia, S. (2007). Using mixed-integer programming to solve power grid blackout problems. *Discrete Optimization*, *4*, 115–141.

Birge, J. R. (1982). The value of the stochastic solution in stochastic linear programs with fixed recourse. *Mathematical Programming*, *24*, 314–325.

Bruninx, K. (2014). A practical approach on scenario generation and & reduction algorithms for wind power forecast error scenarios.

Bryson, K. M., Millar, H., Joseph, A., & Mobolurin, A. (2002). Using formal MS/OR modeling to support disaster recovery planning. *European Journal of Operational Research*, *141*, 679–688.

Campbell, R. J., & Lowry, S. (2012). Weather-related power outages and electric system resiliency. Washington, DC: Library of Congress.

Casari, M., & Wilkie, S. J. (2005). Sequencing lifeline repairs after an earthquake: An economic approach. *Journal of Regulatory Economics*, *27*, 47–65.

Çelik, M., Ergun, Ö., & Keskinocak, P. (2015). The post-disaster debris clearance problem under incomplete information. *Operations Research*, *63*, 65–85.

Chang, L., & Wu, Z. (2011). Performance and reliability of electrical power grids under cascading failures. *International Journal of Electrical Power and Energy Systems*, *33*, 1410–1419.

Chen, J., Lim, C. H., Qian, P. Z., Linderoth, J., & Wright, S. J. (2014). Validating sample average approximation solutions with negatively dependent batches, . arXiv:1404.7208v2.

CNBC (2017). Harvey and Irma economic hit could total $200 billion: Moody's. Available at: https://www.cnbc.com/2017/09/11/harvey-and-irma-economic-hit-could-total-200-billion-moodys.html.

CPLEX, IBM. (2020). CPLEX Optimizer — IBM. https://www.ibm.com/analytics/cplex-optimizer.

de la Torre, L. E., Dolinskaya, I. S., & Smilowitz, K. R. (2012). Disaster relief routing: Integrating research and practice. *Socio-Economic Planning Sciences*, *46*, 88–97. Special Issue: Disaster Planning and Logistics: Part 1.

D'Electricité, L. R. d. T. (2019). RTE - Generation forecast. https://clients.rte-france.com. Available at: https://clients.rte-france.com/lang/an/visiteurs/vie/prod/prevision{_}production.jsp?t=solaire.

Dupačová, J., Gröwe-Kuska, N., & Römisch, W. (2003). Scenario reduction in stochastic programming. *Mathematical Programming*, *95*, 493–511.

Ellis, J., Fisher, D., Longstaff, T., Pesante, L., & Pethia, R. (1997). *Report to the President's Commission on Critical Infrastructure Protection.*. Technical Report Carnegie Mellon University Software Engineering Institute Pittsburgh, PA. Available at: https://apps.dtic.mil/docs/citations/ADA324232.

Escudero, L. F., Garín, M. A., & Unzueta, A. (2017). Scenario cluster Lagrangean decomposition for risk averse in multistage stochastic optimization. *Computers & Operations Research*, *85*, 154–171. URL: http://www.sciencedirect.com/science/article/pii/S0305054817300989.

Executive Office of the President (2011). *A Policy Framework for the 21st Century Grid: Enabling Our Secure Energy Future*. Washington, D.C.: National Science and Technology Council.

Fairbrother, J., Turner, A., & Wallace, S. W. (2019). Problem-driven scenario generation: an analytical approach for stochastic programs with tail risk measure. *Mathematical Programming*, .

Fang, Y., Pedroni, N., & Zio, E. (2016). Resilience-Based Component Importance Measures for Critical Infrastructure Network Systems. *IEEE Transactions on Reliability*, *65*, 502–512.

Fang, Y., Pedroni, N., & Zio, E. (2017). Comparing network-centric and power flow models for the optimal allocation of link capacities in a cascade-resilient power transmission network. *IEEE Systems Journal*, *11*, 1632–1643.

Fang, Y., & Sansavini, G. (2017). Emergence of antifragility by optimum postdisruption restoration planning of infrastructure networks. *Journal of Infrastructure Systems*, *23*, 04017024.

Fang, Y., & Sansavini, G. (2019). Optimum post-disruption restoration under uncertainty for enhancing critical infrastructure resilience. *Reliability Engineering and System Safety*, *185*, 1–11.

FEMA (2017). Historic disaster response to hurricane harvey in texas. Available at: `https://www.fema.gov/news-release/2017/09/22/historic-disaster-response-hurricane-harvey-texas`.

Force, Hurricane Sandy Rebuilding Task Force. (2013). *Hurricane Sandy rebuilding strategy*. US Department of Housing and Urban Development, Washington, DC.

Garay-Sianca, A., & Pinkley, S. G. N. (2021). Interdependent integrated network design and scheduling problems with movement of machines. *European Journal of Operational Research*, *289*, 297–327.

García-Bertrand, R., & Mínguez, R. (2012). Iterative scenario based reduction technique for stochastic optimization using conditional value-at-risk. *Optimization and Engineering*, *15*, 355–380.

Gasser, P., Lustenberger, P., Cinelli, M., Kim, W., Spada, M., Burgherr, P., Hirschberg, S., Stojadinovic, B., & Sun, T. Y. (2019). A review on resilience assessment of energy systems. *Sustainable and Resilient Infrastructure*, (pp. 1–27).

Gomez, C., González, A. D., Baroud, H., & Bedoya-Motta, C. D. (2019). Integrating operational and organizational aspects in interdependent infrastructure network recovery. *Risk Analysis*, *39*, 1913–1929.

González, A. D., Dueñas-Osorio, L., Sánchez-Silva, M., & Medaglia, A. L. (2016). The interdependent network design problem for optimal infrastructure system restoration. *Computer-Aided Civil and Infrastructure Engineering*, *31*, 334–350.

Heitsch, H., & Römisch, W. (2003). Scenario reduction algorithms in stochastic programming. *Computational Optimization and Applications*, *24*, 187–206.

Helbing, D. (2013). Globally networked risks and how to respond. *Nature*, *497*, 51–59. doi:`10.1038/nature12047`.

Henry, D., & Ramirez-Marquez, J. E. (2012). Generic metrics and quantitative approaches for system resilience as a function of time. *Reliability Engineering and System Safety*, *99*, 114–122.

Hollnagel, E., Woods, D. D., & Leveson, N. (2006). *Resilience engineering: Concepts and precepts*. Aldershot, UK: Ashgate Publishing, Ltd.

Homem-de-Mello, T., & Pagnoncelli, B. K. (2016). Risk aversion in multistage stochastic programming: A modeling and algorithmic perspective. *European Journal of Operational Research*, *249*, 188–199.

Horejšová, M., Vitali, S., Kopa, M., & Moriggia, V. (2020). Evaluation of scenario reduction algorithms with nested distance. *Computational Management Science*, *17*, 241–275.

Hosseini, S., Barker, K., & Ramirez-Marquez, J. E. (2016). A review of definitions and measures of system resilience. *Reliability Engineering and System Safety*, *145*, 47–61.

Iloglu, S., & Albert, L. A. (2020). A maximal multiple coverage and network restoration problem for disaster recovery. *Operations Research Perspectives*, 7, 100132. doi:`10.1016/j.orp.2019.100132`.

Karagiannis, G. M., Chondrogiannis, S., Krausmann, E., & Turksezer, Z. I. (2017). *Power grid recovery after natural hazard impact*. Technical Report EUR 28844 EN Luxembourg.

Kasaei, M., & Salman, F. S. (2016). Arc routing problems to restore connectivity of a road network. *Transportation Research Part E: Logistics and Transportation Review*, *95*, 177–206.

Kleywegt, A. J., Shapiro, A., & Homem-de-Mello, T. (2002). The sample average approximation method for stochastic discrete optimization. *SIAM Journal on Optimization*, *12*, 479–502.

Krokhmal, P., Palmquist, J., & Uryasev, S. (2002). Portfolio optimization with conditional value-at-risk objective and constraints. *Journal of risk*, *4*, 43–68.

Lee II, E. E., Mitchell, J. E., & Wallace, W. A. (2007). Restoration of services in interdependent infrastructure systems: A network flows approach. *IEEE Transactions on Systems, Man, and Cybernetics, Part C (Applications and Reviews)*, *37*, 1303–1317.

Li, Y., & Lence, B. J. (2007). Estimating resilience for water resources systems. *Water Resources Research*, *43*, 1–11.

Luo, H., Alkhaleel, B. A., Liao, H., & Pascual, R. (2020). Resilience improvement of a critical infrastructure via optimal replacement and reordering of critical components. *Sustainable and Resilient Infrastructure*, (pp. 1–21).

Manuel, J. (2013). The long road to recovery: Environmental health impacts of hurricane sandy.

Matisziw, T. C., Murray, A. T., & Grubesic, T. H. (2010). Strategic network restoration. *Networks and Spatial Economics*, *10*, 345–361.

Mete, H. O., & Zabinsky, Z. B. (2010). Stochastic optimization of medical supply location and distribution in disaster management. *International Journal of Production Economics*, *126*, 76–84. Improving Disaster Supply Chain Management – Key supply chain factors for humanitarian relief.

Morales, J. M., Pineda, S., Conejo, A. J., & Carrión, M. (2009). Scenario reduction for futures market trading in electricity markets. *IEEE Transactions on Power Systems*, *24*, 878–888.

Morshedlou, N. (2018). *Adaptive and Restorative Capacity Planning for Complex Infrastructure Networks: Optimization Algorithms and Applications*. Ph.D. thesis University of Oklahoma.

Motter, A. E., & Lai, Y.-C. (2002). Cascade-based attacks on complex networks. *Physical Review E*, *66*.

Noyan, N. (2012). Risk-averse two-stage stochastic programming with an application to disaster management. *Computers & Operations Research*, *39*, 541–559.

Nurre, S. G., Cavdaroglu, B., Mitchell, J. E., Sharkey, T. C., & Wallace, W. A. (2012). Restoring infrastructure systems: An integrated network design and scheduling (INDS) problem. *European Journal of Operational Research*, *223*, 794–806.

Nurre, S. G., & Sharkey, T. C. (2014). Integrated network design and scheduling problems with parallel identical machines: Complexity results and dispatching rules. *Networks*, *63*, 306–326.

O'Donnell, K. (2013). Critical infrastructure resilience: Resilience thinking in australia's federal critical infrastructure protection policy. *Salus Journal*, *1*, 13.

Odyssee-Mure (2020). EU household energy consumption. Available at: `https://www.odyssee-mure.eu/publications/efficiency-by-sector/households/household-eu.pdf`.

Ouyang, M., & Wang, Z. (2015). Resilience assessment of interdependent infrastructure systems: With a focus on joint restoration modeling and analysis. *Reliability Engineering and System Safety*, *141*, 74–82.

Özdamar, L., & Ertem, M. A. (2015). Models, solutions and enabling technologies in humanitarian logistics. *European Journal of Operational Research*, *244*, 55–65.

Pineda, S., & Conejo, A. (2010). Scenario reduction for risk-averse electricity trading. *IET Generation, Transmission & Distribution*, *4*, 694.

Executive Office of the President, Council of Economic Advisers. (2013). *Economic Benefits of Increasing Electric Grid Resilience to Weather Outages*. Washington, D.C.: The Council.

Python (2020). Python.org. https://www.python.org/.

Rachev, S. T. (1991). *Probability metrics and the stability of stochastic models, Scenario*. Chichester New York: Wiley.

Rahmaniani, R., Crainic, T. G., Gendreau, M., & Rei, W. (2017). The benders decomposition algorithm: A literature review. *European Journal of Operational Research*, *259*, 801–817.

Rockafellar, R. T., & Uryasev, S. (2000). Optimization of conditional value-at-risk. *The Journal of Risk*, *2*, 21–41.

Rose, A. (2007). Economic resilience to natural and man-made disasters: Multidisciplinary origins and contextual dimensions. *Environmental Hazards*, *7*, 383–398.

Sharkey, T. C., Cavdaroglu, B., Nguyen, H., Holman, J., Mitchell, J. E., & Wallace, W. A. (2015). Interdependent network restoration: On the value of information-sharing. *European Journal of Operational Research*, *244*, 309–321.

Sharkey, T. C., Pinkley, S. G. N., Eisenberg, D. A., & Alderson, D. L. (2020). In search of network resilience: An optimization-based view. *Networks*, *77*, 225–254.

Vugrin, E. D., Turnquist, M. A., & Brown, N. J. (2014). Optimal recovery sequencing for enhanced resilience and service restoration in transportation networks. *International Journal of Critical Infrastructures*, *10*, 218–246.

White House (2013). Presidential Policy Directive/PPD-21 : Critical Infrastructure Security and Resilience. Office of the Press Secretary: Washington, DC.

Wyss, G. D., & Jorgensen, K. H. (1998). A User ' s Guide to LHS : Sandia's Latin Hypercube Sampling Software Acknowledgments. *Distribution*, (p. 88).

Xu, N., Guikema, S. D., Davidson, R. A., Nozick, L. K., Çağnan, Z., & Vaziri, K. (2007). Optimizing scheduling of post-earthquake electric power restoration tasks. *Earthquake Engineering and Structural Dynamics*, *36*, 265–284.

Zamuda, C., Mignone, B., Bilello, D., Hallett, K., Lee, C., Macknick, J., Newmark, R., & Steinberg, D. (2013). U.S. energy sector vulnerabilities to climate change and extreme weather, .

Zhang, C., Kong, J.-j., & Simonovic, S. P. (2018). Restoration resource allocation model for enhancing resilience of interdependent infrastructure systems. *Safety Science*, *102*, 169–177.

Zio, E. (2016). Challenges in the vulnerability and risk analysis of critical infrastructures. *Reliability Engineering and System Safety*, *152*, 137–150.

Appendix A

A.1. Model adaptation for the power network

The general flow-based model introduced in this paper assumes that the flow in the network can be directly controlled, which is not the case for power infrastructure networks (Bienstock & Mattia, 2007). The DC model is a commonly used linear approximation of the power grid to model its operations, especially the power transmission network (Bienstock & Mattia, 2007; Nurre et al., 2012). The DC model includes decision variables (i.e., the phase angles) for all the nodes in the network. The flow on edge $\{i, j\}$ is then a function of the phase angles of nodes i and j along with the reactance of the edge $\{i, j\}$. The reactance, b_{ij}, of the edge is dependent on its length and the voltage levels. By defining θ_i for $i \in V$ as the phase angle of node i, the flow on edge $\{i, j\}$ for a given scenario is determined by:

$$b_{ij} f_{ij} = \theta_i - \theta_j \tag{A.1}$$

Note that both the phase angle variables and the edge flow variables are unrestricted in the DC model. A negative flow on edge $\{ij\}$ corresponds to power flowing from node j to node i. Therefore, it is necessary to incorporate the constraints given by Equation (A.1) into the optimization problem (9)–(30). We define variables $\theta_i(t)$ for $i \in V$ and $t \in \{1 \dots, T\}$ for the phase angle of node i in time period t. Then, the DC flow is incorporated by adding two constraints controlling flow on each edge along with (14):

$$b_{ij} f_{ij\omega}(t) \leq \theta_{i\omega}(t) - \theta_{j\omega}(t) + M\left[1 - s_{ij\omega}(t)\right], \forall ij \in E, \forall t \in \{1, \dots, T\}, \forall \omega \in \Omega_s \tag{A.2}$$

$$b_{ij} f_{ij\omega}(t) \geq \theta_{i\omega}(t) - \theta_{j\omega}(t) - M\left[1 - s_{ij\omega}(t)\right], \forall ij \in E, \forall t \in \{1, \dots, T\}, \forall \omega \in \Omega_s \tag{A.3}$$

Therefore, whenever $s_{ij\omega}(t) = 1$, constraints (A.2) and (A.3) will make sure that the DC flow satisfies Equation (A.1) for edge $\{i, j\}$ in time period t. In addition, Constraints (A.2) and (A.3) are added to the optimization problem (9)–(30) and to each scenario-related subproblem from the proposed Benders decomposition.

A.2. Optimality gap calculation

Regarding the relative optimality gap of the stochastic optimization models, we note that the optimality gap using the resilience measure (or loss of resilience) by Fang et al. (2016) is inflated given a constant term in the objective function's numerator representing either the negative summation of the aggregated system performance measure (flow in our case) in the disrupted state: $-\sum_{t=1}^{t=T} \varphi(0)$ for a maximization problem or the summation of aggregated system flow over time in the nominal state: $\sum_{t=1}^{t=T} \varphi(t_0)$ for a resilience loss minimization problem. For example, if the cumulative sum of flow $\forall t \in \{1 \dots T\}$ is 100, $\sum_{t=1}^{t=T} \varphi(0) = 70$ and $\sum_{t=1}^{t=T} \varphi(t_0) = 120$, the resilience objective function solution ($\widehat{Obj}$) will be 0.60 and if we assume that the upper bound on the cumulative flow is 115, the upper bound on resilience (Obj^{UB}) will be 0.90; thus, if we calculate the optimality gap by: $\left(\frac{Obj^{UB}}{\widehat{Obj}}\right) - 1$, it will be estimated as 50.00% where the gap in terms of the aggregated flow: $\left(\frac{\text{Aggregated Flow}^{UB}}{\widehat{\text{Aggregated Flow}}}\right) - 1$, which is the term to be maximized, is 15.00%. Based on that, we use from this point onward an adjusted optimality gap calculated using: $\left(\frac{Obj^{UB} + \frac{T\varphi(0)}{T(\varphi(t_0) - \varphi(0))}}{\widehat{Obj} + \frac{T\varphi(0)}{T(\varphi(t_0) - \varphi(0))}}\right) - 1$ for a maximization problem and:

$\left(\frac{\frac{T\varphi(t_0)}{T(\varphi(t_0)-\varphi(0))}-Obj^{LB}}{\frac{T\varphi(t_0)}{T(\varphi(t_0)-\varphi(0))}-\widehat{Obj}}\right)-1$ for a minimization objective to eliminate the impact of constant terms on the gap estimation of the aggregated flow. In Table 2, we compare the proposed Benders algorithm to the standard CPLEX solver. The optimalty gap for the Benders implementation is found using: $\left(\frac{\frac{T\varphi(t_0)}{T(\varphi(t_0)-\varphi(0))}-LB}{\frac{T\varphi(t_0)}{T(\varphi(t_0)-\varphi(0))}-\widehat{Obj}}\right)-1$ where LB is the lower bound representing the optimal objective function value of the master problem at the last iteration of the algorithm before termination. For the CPLEX solver, we use the reported best lower bound on the objective function Obj^{LB}_{solver} and the best available objective value $\widehat{Obj}_{solver}$ reported by CPLEX: $\left(\frac{\frac{T\varphi(t_0)}{T(\varphi(t_0)-\varphi(0))}-Obj^{LB}_{solver}}{\frac{T\varphi(t_0)}{T(\varphi(t_0)-\varphi(0))}-\widehat{Obj}_{solver}}\right)-1$ to calculate the optimality gap.

Appendix B

B.1. Maps of failed components for numerical studies

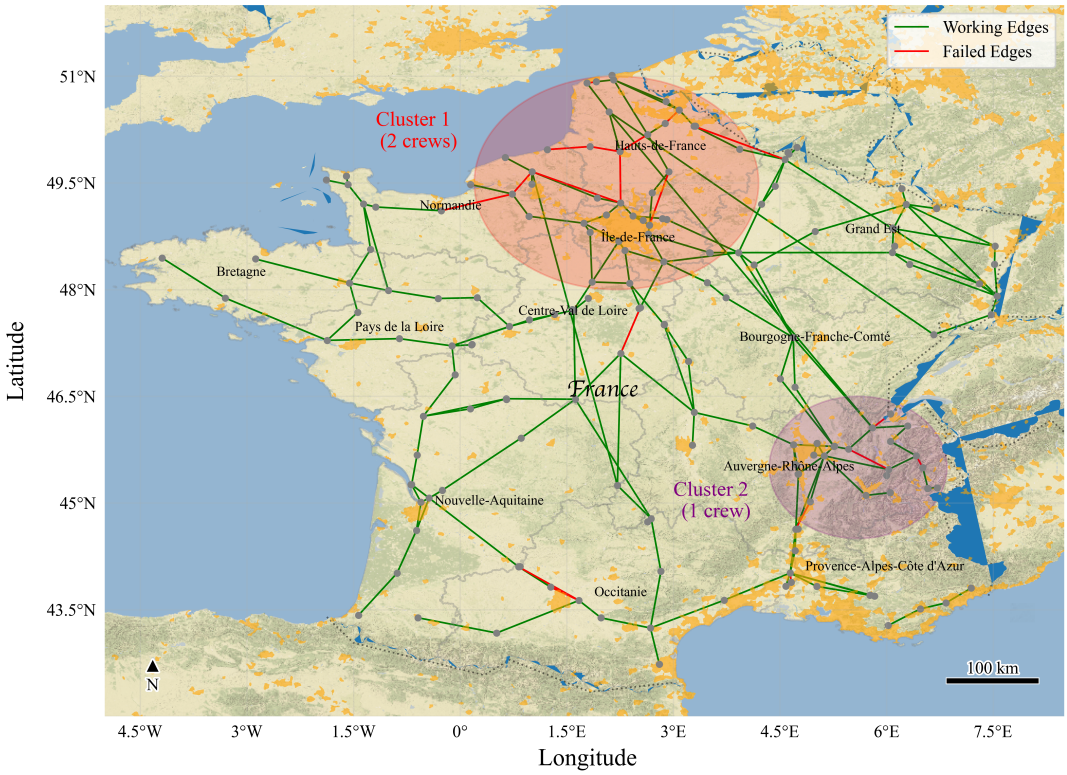

Figure 11: Case 1: Distribution of random failures

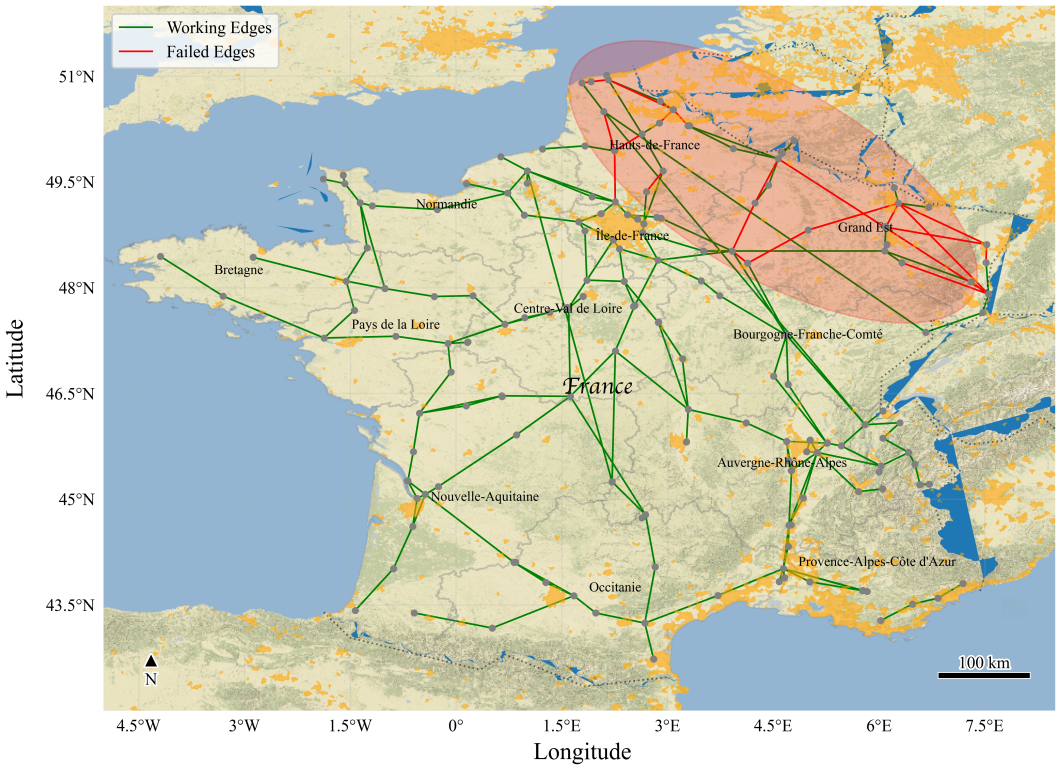

Figure 12: Case 2: Distribution of cascading failures

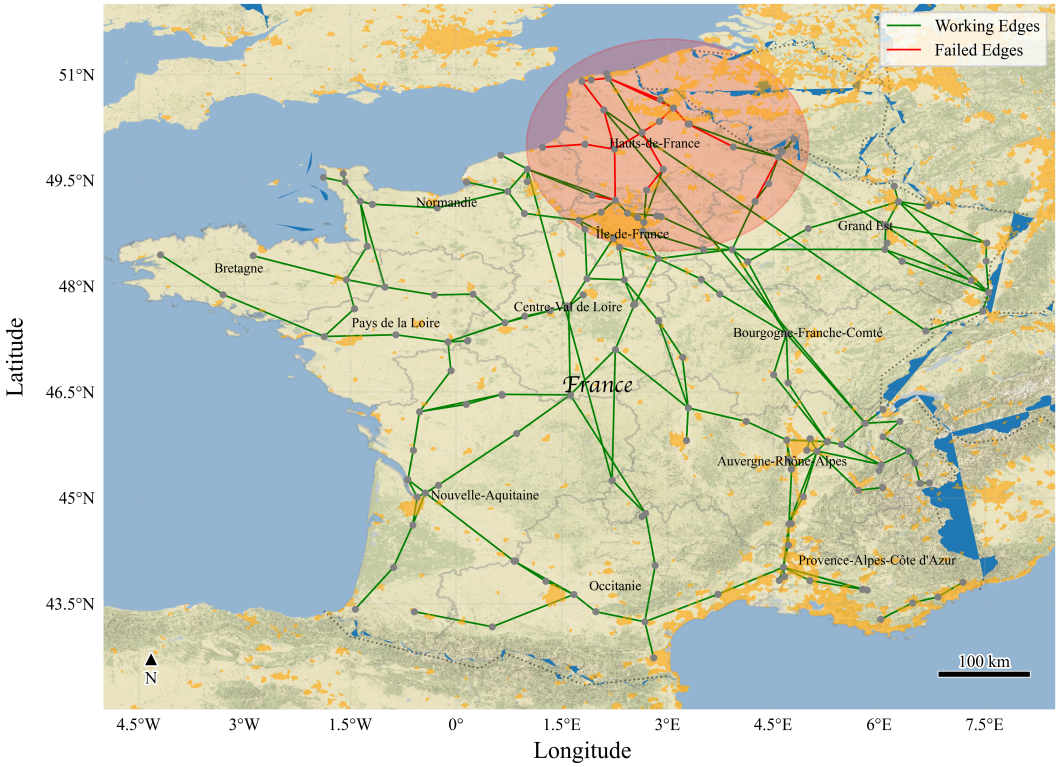

Figure 13: Case 3: Distribution of spatial failures

B.2. Sample of optimal solution routing under deterministic travel times

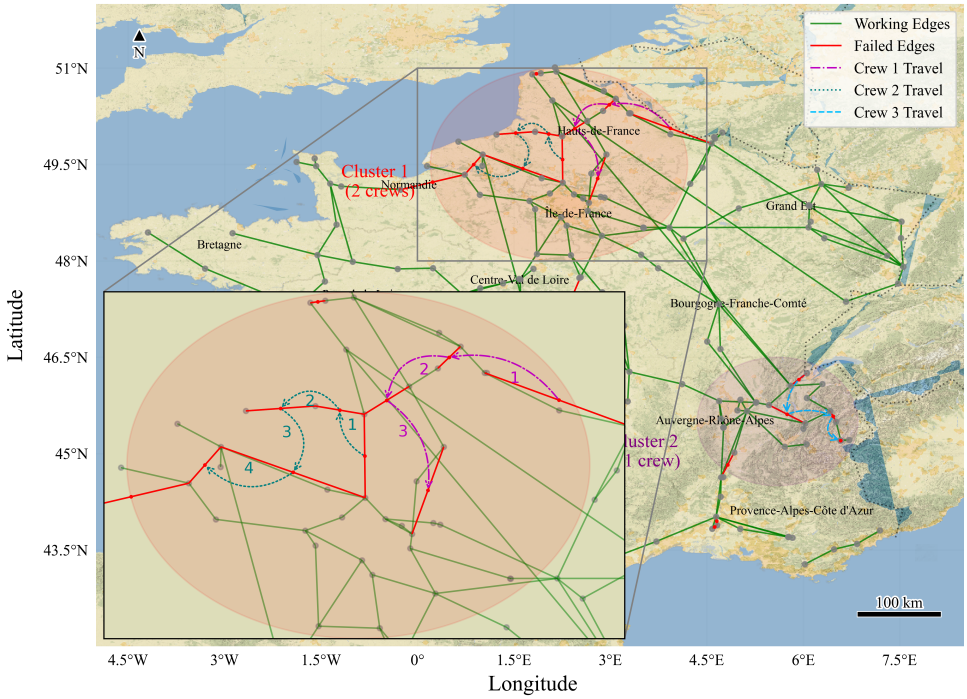

Figure 14: Case 1-b (Random Failures with Deterministic Travel Times): Optimal routing for crews 1 and 2

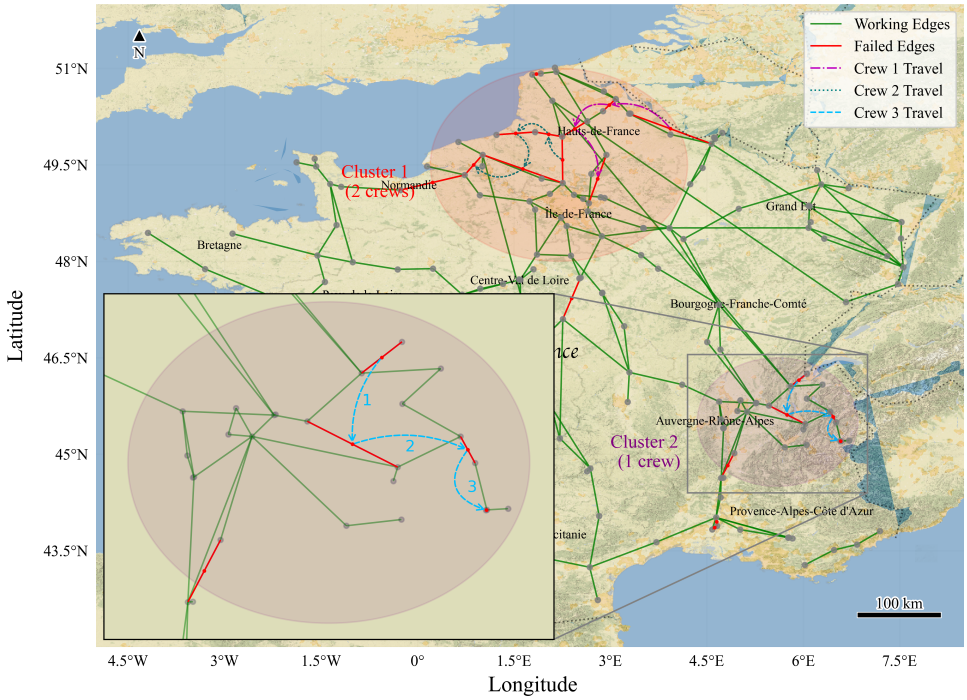

Figure 15: Case 1-b (Random Failures with Deterministic Travel Times): Optimal routing for crew 3

B.3. Resilience curves under different considerations of travel times

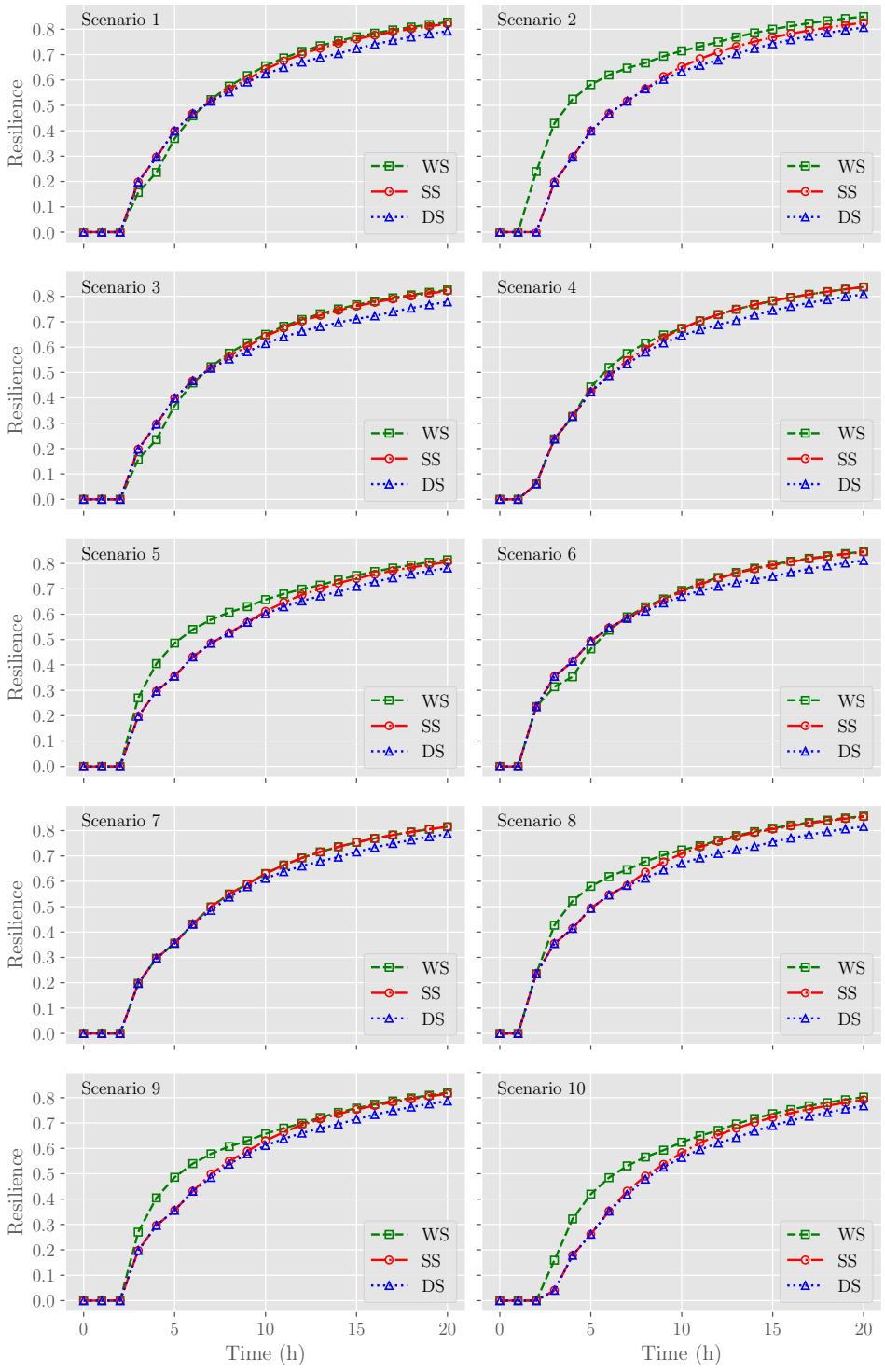

Figure 16: Case 1-c (Random Failures with Random Travel Times): Comparison of resilience curves under different solution plans for the reduced 10 scenarios

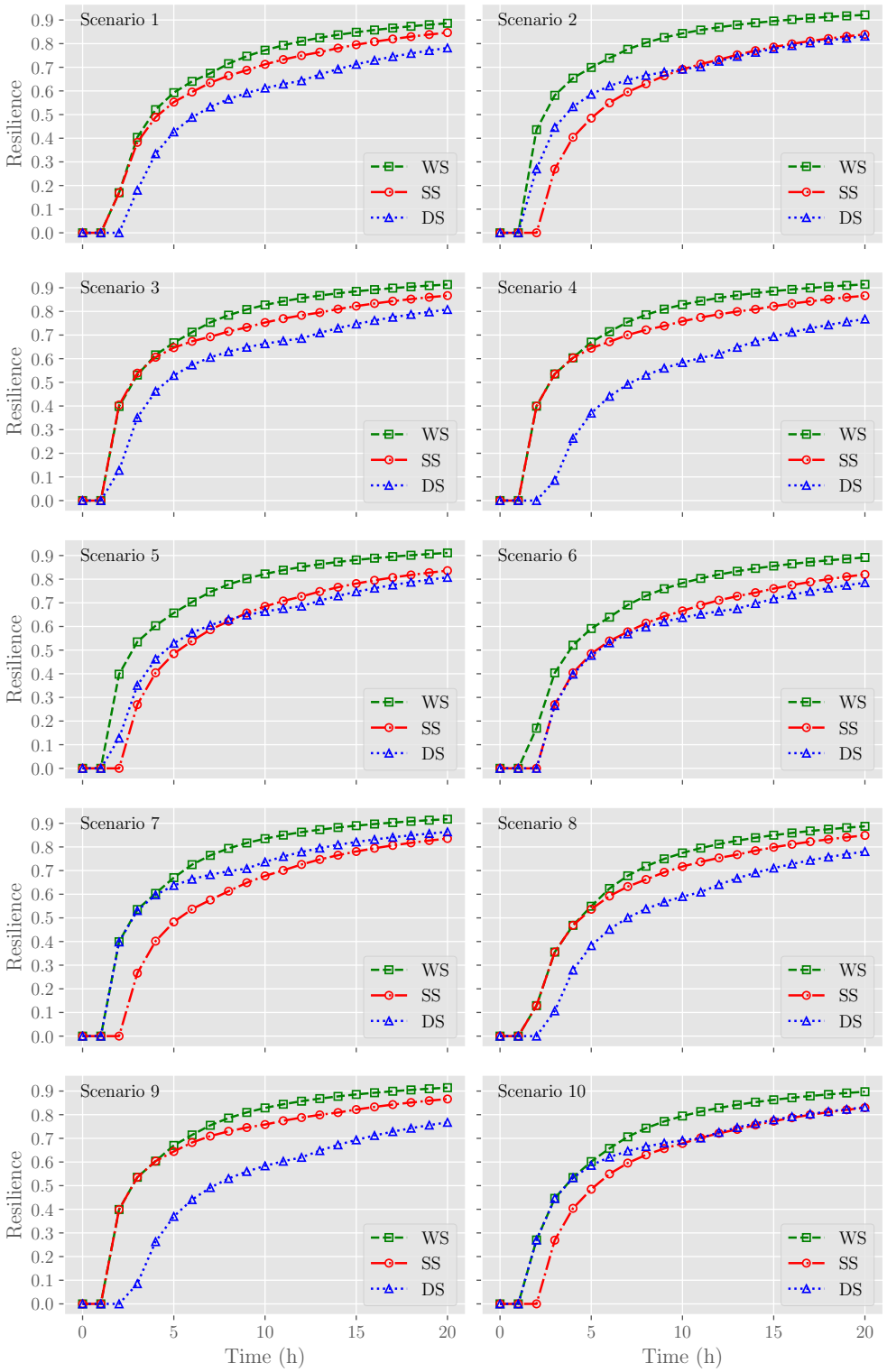

Figure 17: Case 2-c (Cascading Failures with Random Travel Times): Comparison of resilience curves under different solution plans for the reduced 10 scenarios

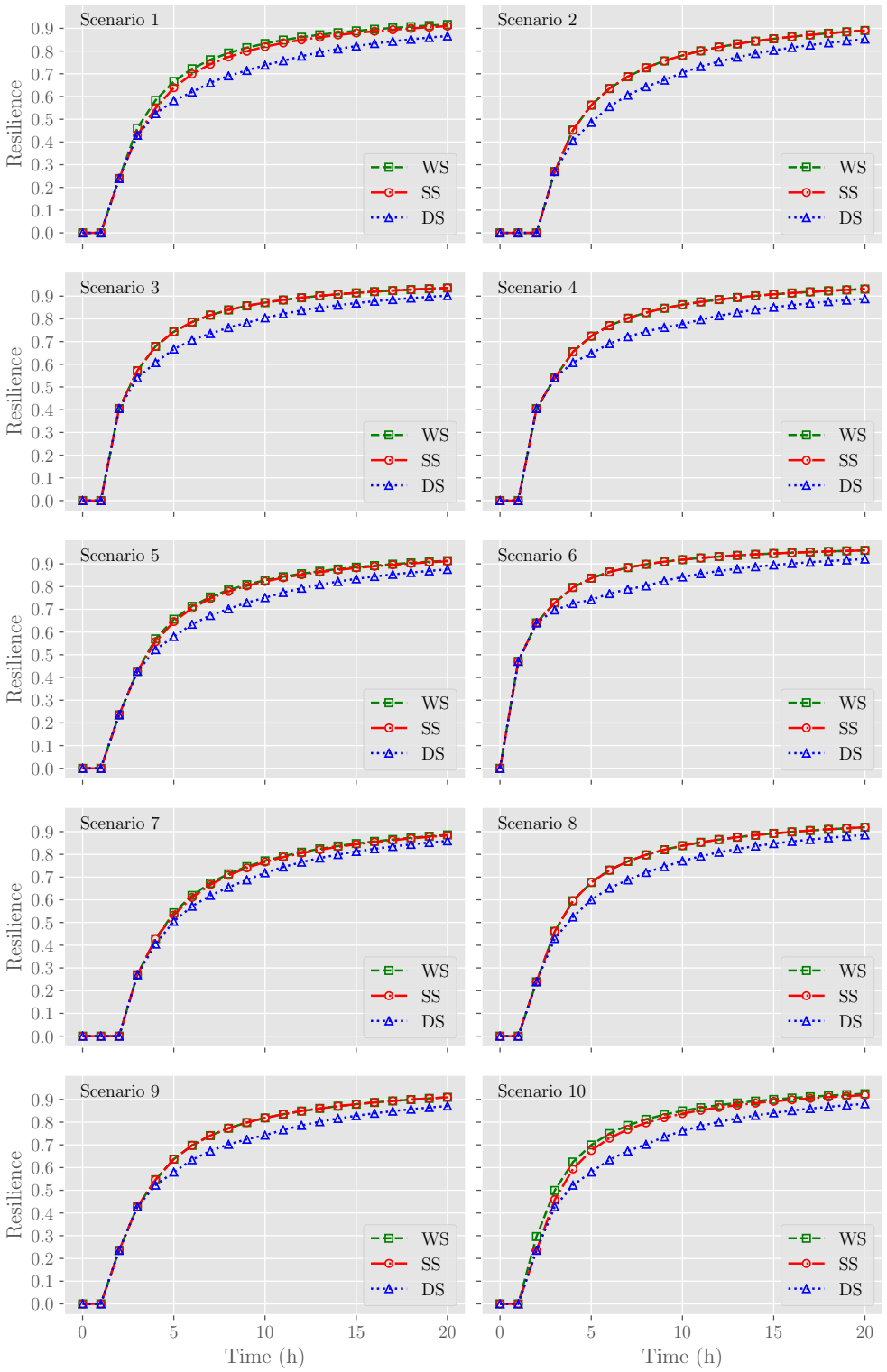

Figure 18: Case 1-a (Random Failures without Travel Times): Comparison of resilience curves under different solution plans for the reduced 10 scenarios

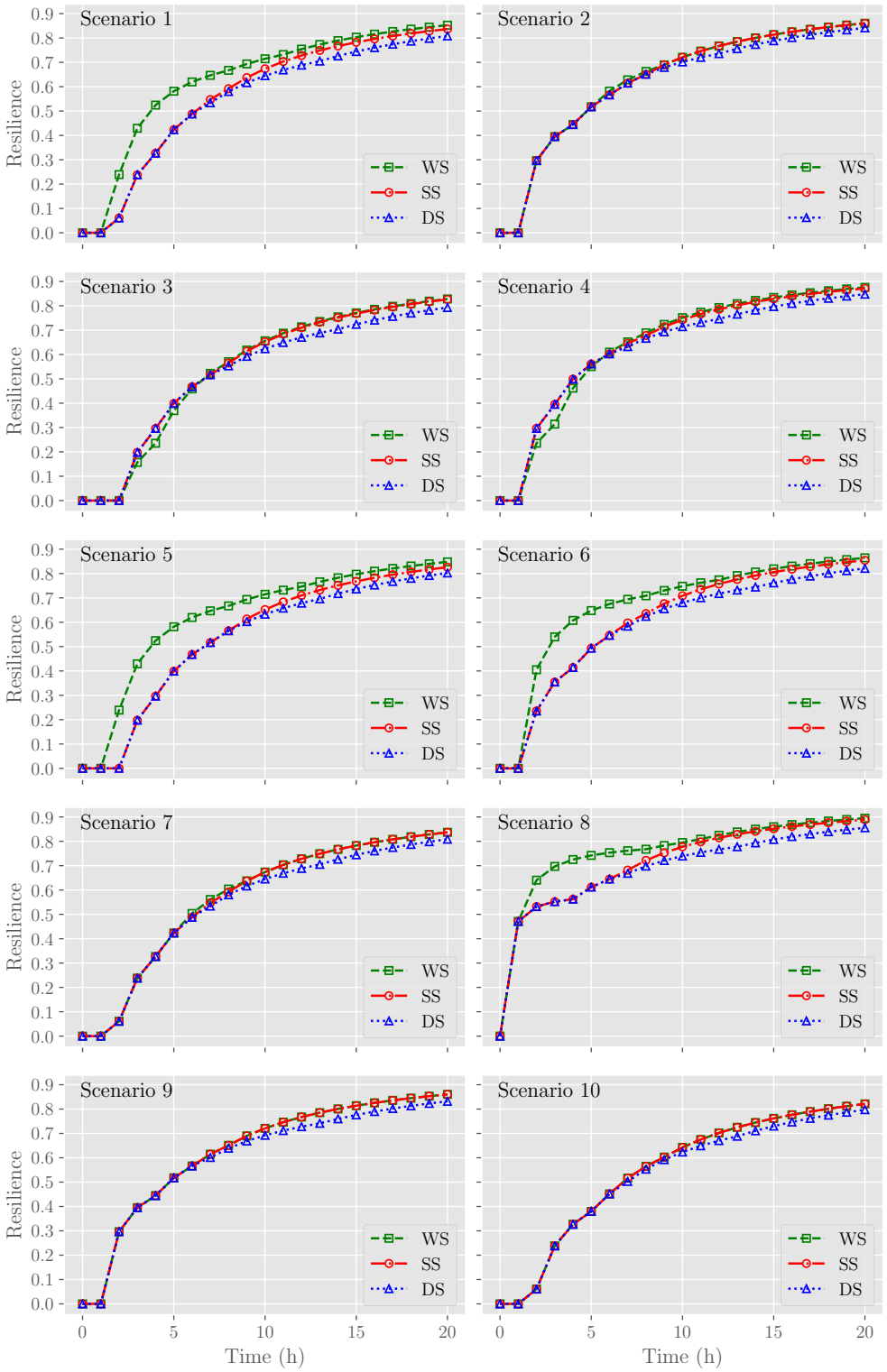

Figure 19: Case 1-b (Random Failures with Deterministic Travel Times): Comparison of resilience curves under different solution plans for the reduced 10 scenarios

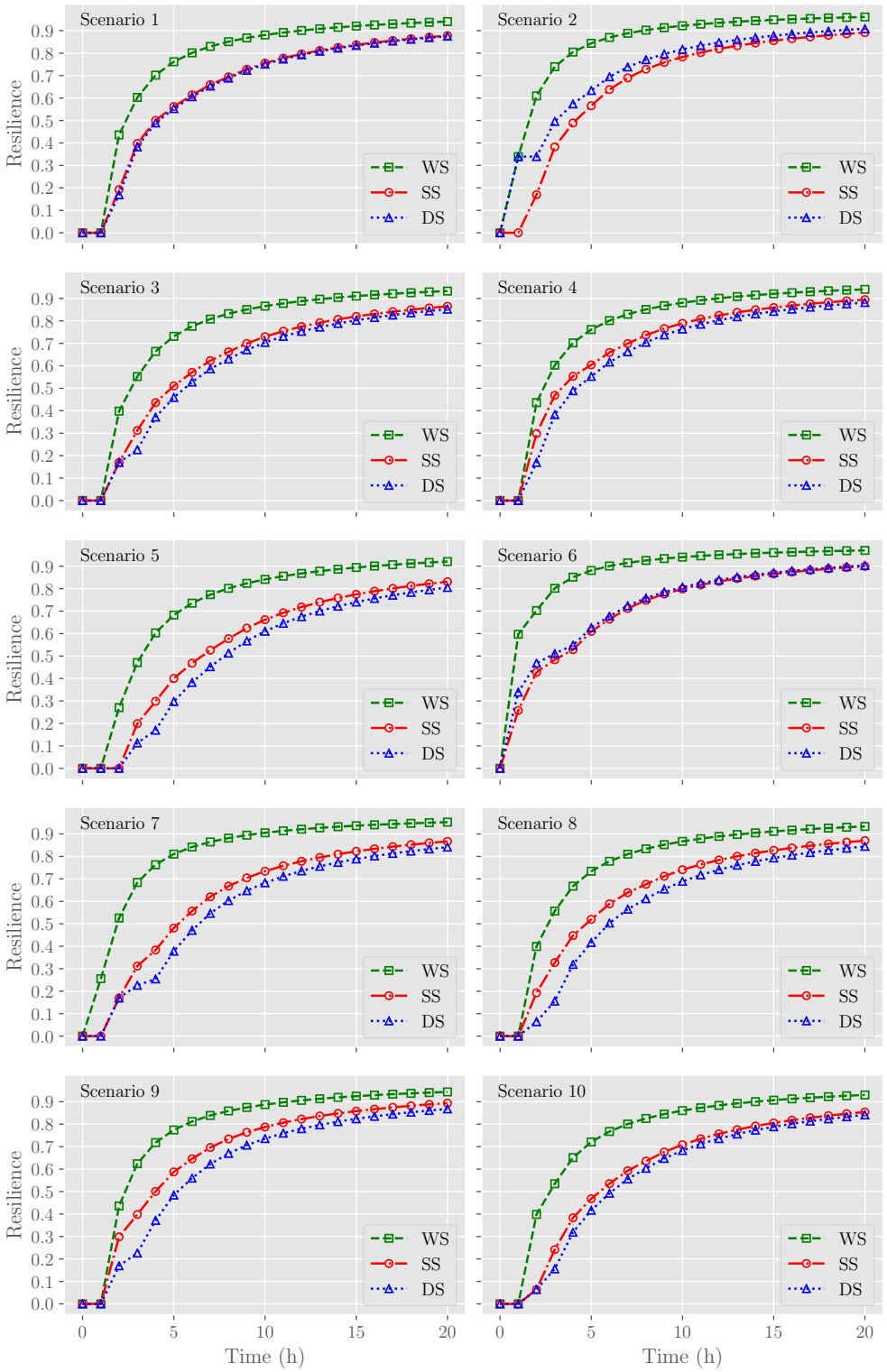

Figure 20: Case 2-a (Cascading Failures without Travel Times): Comparison of resilience curves under different solution plans for the reduced 10 scenarios

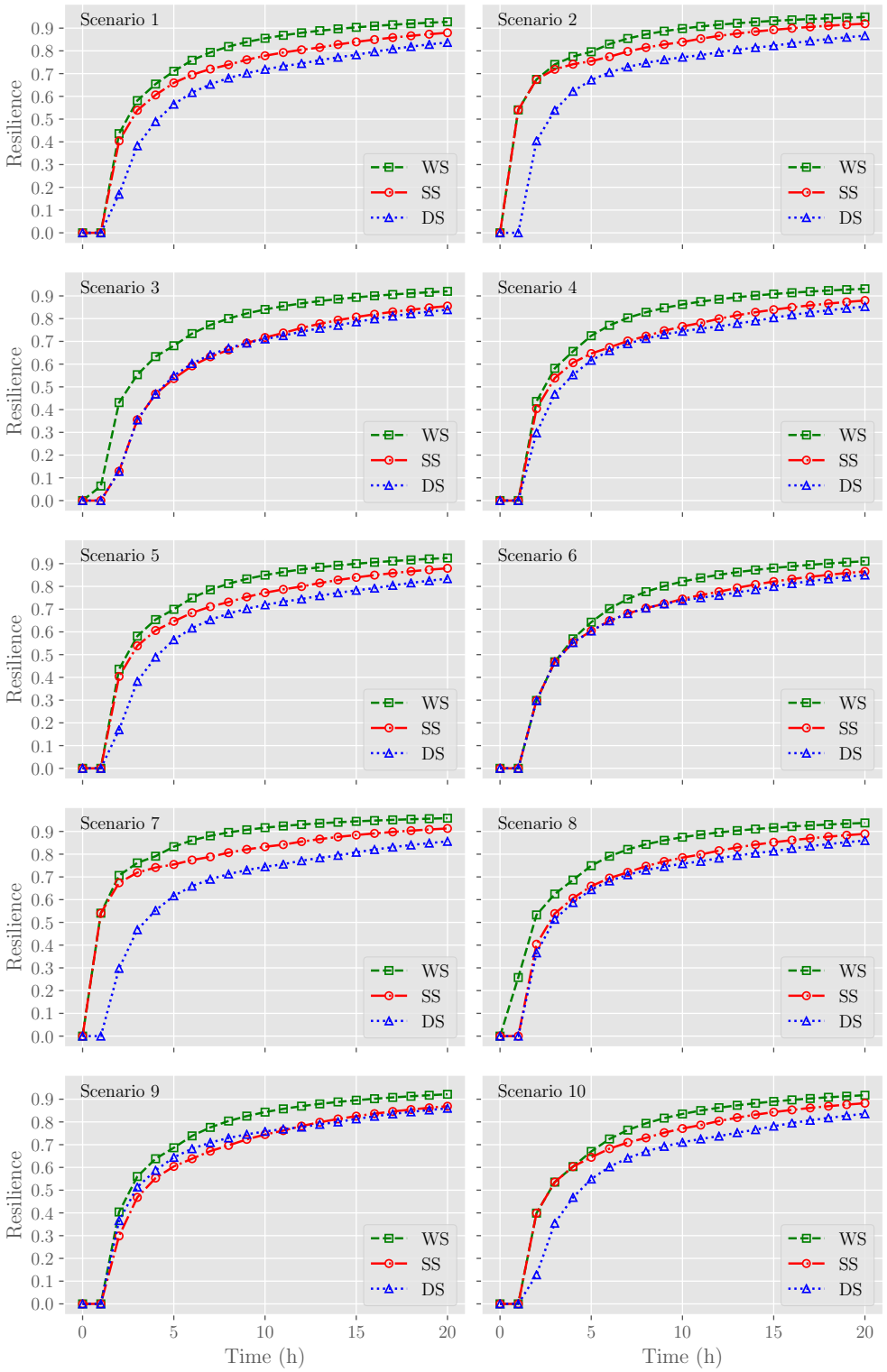

Figure 21: Case 2-b (Cascading Failures with Travel Times): Comparison of resilience curves under different solution plans for the reduced 10 scenarios